There are 10 types of people in this world. Those that understand binary and those that don't.

– Unknown.

University of Alberta

NASAL FILTRATION IN INFANTS BY IMPACTION

by

John Storey-Bishoff ©

A thesis submitted to the Faculty of Graduate Studies and Research in partial fulfillment of the requirements for the degree of **Master of Science**.

Department of Mechanical Engineering

Edmonton, Alberta
Fall 2008

Library and
Archives Canada

Published Heritage
Branch

395 Wellington Street
Ottawa ON K1A 0N4
Canada

Bibliothèque et
Archives Canada

Direction du
Patrimoine de l'édition

395, rue Wellington
Ottawa ON K1A 0N4
Canada

Canada

To my parents who were my early teachers,
and to my wife from whom I continue to learn.

Abstract

In vitro measurements of particle filtration were made for nasal geometries of eleven infants aged three months to 18 months. The geometries were obtained from computed tomography (CT) scans of seven male and four female infants and replicas were built using rapid prototyping. Particles ranging in aerodynamic diameter from 0.8 μm to 5.3 μm were passed through these replicas with simulated tidal breathing. Filtration was determined from particle counts upstream and downstream of the models. Mathematical fits were constructed to predict the measured deposition based on the relevant parameters. The fractional deposition is found to depend on the Reynolds number of the flow (Re), the particle Stokes number (Stk) and an airway dimension D defined as airway volume divided by airway surface area.

Acknowledgements

Table of Contents

List of Tables

List of Figures

Chapter 1

Introduction

1.1 Context

An aerosol is defined as a suspension of particles in a gas. In the current work we are particularly interested in suspensions in air which are then inhaled by people. These aerosol particles can take many forms and can be characterized in a number of ways. The particles can be solid or liquid, spherical or irregular, dense or not dense, porous or uniform, of a single size or of a wide range of sizes. Aerosols can also have large aspect ratios, as in the case of asbestos, which result in interesting aerodynamic properties. Aerosols can be present in the surroundings naturally or as a side effect of human activity, in which case they are often referred to as environmental aerosols. Aerosols can also be purposefully introduced into the air we breath to produce a therapeutic effect and may contain drugs in which case they are often called pharmaceutical aerosols (especially if they are commercially prepared).

Aerosols which are inhaled into the airway but then immediately exhaled usually have limited effect compared to those which are retained. Since the human airway is quite heterogeneous the effect of an aerosol which is inhaled but not exhaled will depend a great deal on where it comes to rest. The fate of a particle deposited in the nasal vestibule will be quite different from that of a particle deposited in the alveoli of the lung.

Many pharmaceutical aerosols are targeted at the lungs to treat chronic diseases such as asthma and cystic fibrosis. For these medications to be effective they must

penetrate through many branchings of the airway to make it deep into the lung. Many aerosol delivery devices, as well as the particles that make up the aerosols they deliver, are designed with this penetration in mind.

Inhalation therapy has a documented history dating back more than 4000 years [3] and is likely much older than that. Methods of therapy have included direct inhalation of medicinal smoke, plant vapours, and steams; the use of nebulizer and atomizers; metered dose inhalers with and without holding chambers and face masks; ultra-sonic nebulizers and dry powder inhalers [3].

There has also been a great deal of research looking at aerosol deposition in humans from the workplace health and safety perspective. This is especially of interest in cases where there may be exposure to inhalable radioactive particles.

The lungs have a tremendous amount of surface area in order to facilitate gas exchange and are a significant interface between the body and the outside world. This makes them an important avenue of exposure to environmental hazards. Much of this occupational health and safety research has focussed on adults since occupational hazards are chiefly borne by adults.

Most of the research in aerosol deposition can be considered to fall into four veins:

- Theoretical work which extends well understood and easily modeled situations such as deposition in straight tubes to create models of aerosol behaviour in the human airway[43].

- Computational fluid dynamics (CFD) which is applied to geometries of differing complexity to calculate the expected flow patterns and aerosol deposition. There is a full spectrum of modeling detail that can be captured here and this is an area which continues to benefit from advances in computer hardware and modeling approaches [34, 30].

- *in vitro* work which measures aerosol deposition experimentally in model geometries of different complexity [44, 27, 28].

2

- *in vivo* work which measures depositions experimentally in humans or animal models directly [1, 2].

Both the nasal and oral airways play important roles depending on the mode of breathing. The human nasal airway has a reasonably complex geometry with regions of recirculating flows. It is currently beyond the ability of theoretical or CFD methods to accurately predict the deposition of aerosol in these kinds of geometries in a tractable amount of time [34].

Related studies of nasal lesions created by toxic gases or vapours as discussed by Morgan and Monticello [35] and experimental characterization of nasal airflow patterns such as Hopkins et al. [16] help in understanding nasal aerosol deposition. A knowledge of air flow patterns in the nasal airway is required to understand local deposition in that geometry.

Studies of aerosol filtration by the oral airway have been performed by Grgic et al. [14] and others and is reasonably well understood in adults. The focus of the current work is nasal filtration of aerosol in the very young.

1.2 Nasal Aerosol Deposition

Children below an age of 7-8 years of age are unable to voluntarily perform the maneuvers required to use aerosol delivery devices designed for adults [22] such as the direct use of metered dose inhalers. Aerosol therapy for children younger than this is usually performed by free breathing through a face mask with adult assistance. Children below an age of 4 to 6 months are physiologically adapted to be able to breath through their noses while breast feeding. These children exclusively breath through their noses[41] so aerosol delivered to the lungs must pass through the nasal airway. Despite the importance of the nasal route for infant pharmaceutical aerosol delivery, deposition of micrometer-sized aerosol in the nasal airways of infants has not been well studied.

The nose has many functions. These functions include filtration of dusts and other particles, heating and humidification of inhaled air and the delivery of air to

the olfactory bulb for smelling. A good introductory discussion of the anatomy and functions of the nose is that by Mygind et al. [36]. Because the nose acts as a filter, the amount of aerosol that makes its way through the nose into the lungs depends on the ability of the nose to filter particles during breathing.

The objective of this work is to be able to predict the fraction of a given aerosol which would make it past a child's nasal passages, larynx and into their trachea if it is inhaled nasally under known breathing conditions. This is useful information when studying either environmental aerosols or pharmaceutical aerosols.

Briefly speaking the nasal airway is composed of two major air paths and a number of sinuses. The two main airways are separated by the nasal septum which runs along the centreline of the face and maintains a separation between the flows from the nares or exterior boundary of the nostril up to the nasopharynx where a single conducting airway is formed. Sequentially the conducting nasal airway can be divided into the nasal vestibule, the nasal cavity and the nasopharynx which is connected to the oropharynx. The nasal vestibule is separated from the nasal cavity by a constriction formed by the limen nasi. This constriction is called the nasal valve or internal ostium. The two airways continue as narrow vertical passages until the concha or turbinates are encountered. These are fleshy appendages attached to the outside walls of the nasal cavity. In most people there are three such turbinates named from the floor of the nasal cavity upwards as the inferior, middle and superior turbinates. The superior turbinates can be quite small in some individuals and do not extend as far forwards towards the nares. The air-spaces of the nasal cavity are divided by these turbinates with the space below the inferior turbinate being called the inferior meatus, that below the middle turbinate being called the middle meatus and that below the superior turbinate called the superior meatus. These features are shown in an anatomical sagital view of the outer wall of the nasal cavity, Figure 1.1, taken from Lang[32]. Many of these features can also be seen in the coronal magnetic resonance imaging slices in Figure 1.2.

It is worth noting that the age group of interest will not have developed nasal hairs which occupy the nasal vestibule in adults and can act as a filter of very course

4

Figure 1.1: Sagital nasal section of adult, showing: 3. Middle turbinate 6. Nasal vestibule 7. Linem nasi 8. Start of inferior turbinate 10. Superior turbinate. (From Johannes Lang In: Clinical Anatomy of the Nose, Nasal Cavity and Paranasal Sinuses. New York: Thieme Medical Publishers, Inc.; 1989: p. 43. Reprinted by permission.)

particles.

There are a number of sinuses surrounding the nasal cavity. Directly behind the forehead is the frontal sinus. The ethmoidal cells lie directly above the nasal septum. The maxillary sinuses lie to the left and right of nasal cavity. A more detailed discussion of nasal anatomy can be found in Lang[32]. Particular details of the changes in the nasal airway with development during infancy can be found by Djupesland and Lyholm[9].

Infancy is, naturally, a time of rapid change and development. Average life expectancy in Canada is over 80 years [18]. The current work concentrates on infants below the age of two years which represents a small fraction of a person's
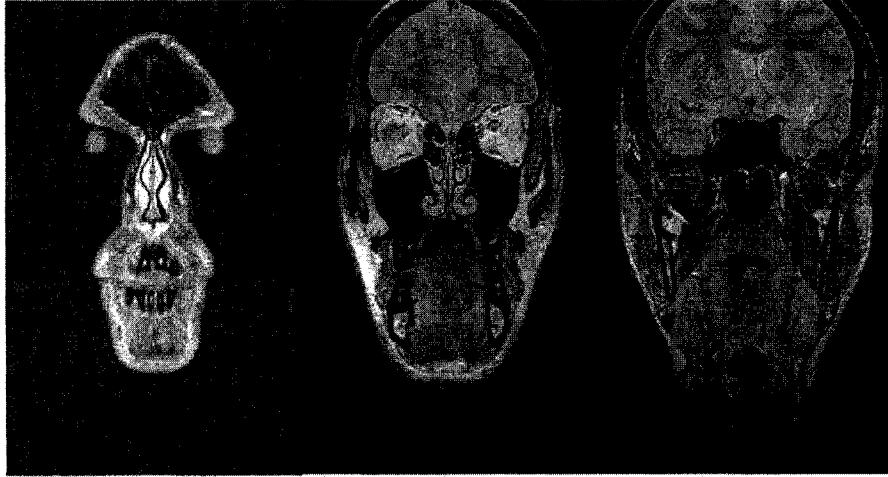
Figure 1.2: Coronal sections showing, from left to right: 1. anterior section of nasal cavity 2. turbinates, maxillary sinuses and ethmoidal cells 3. nasopharynx

lifetime but a great deal of change[9]. Respiratory infections and problems are also a very common cause for infants to be brought to the emergency rooms in Canada. Many acute health conditions can have lasting impacts so effective treatment of infants is very important. Chronic asthma also is increasing in North America and is a disease commonly treated by pharmaceutical aerosol therapy.

Ideally, *in vivo* experiments would be performed to measure nasal and lung deposition in the child of interest in the disease state of interest. This information could then be used to accurately provide appropriate dosage of medication. This characterization requires special equipment and setup which is not generally available as part of regular health care and may present risks to the patient. An alternative would be to make *in vivo* nasal deposition measurements on a large number of children in order to be able to generalize to a specific patient. Unfortunately, some of the most accurate methods of measuring aerosol deposition *in vivo* require the use of radioactive markers which pose a health risk to subjects. These *in vivo* studies also have the disadvantages of being expensive and having a parameter space that is difficult to control. For instance adult volunteers can modify their breathing patterns if requested while infant subjects will not be able to. This will make it hard to

experiment with the effect of different breathing patterns on nasal deposition. The children are also continuously growing so that experiments must be performed over a short time period if the geometry is to be kept fixed.

As an alternative the present study employs realistic nasal airway models to perform *in vitro* experiments in a controlled laboratory setting. It is hoped that these results can be generalized to infants requiring pharmaceutical aerosol therapy and to those exposed to environmental aerosols.

It should also be remembered that the same lung dosage of a medication may have different efficacy in different individuals so that an exact estimation of lung dose may not, in itself, allow the prediction of the desired effect from the aerosol generating device.

1.3 Background Theory

A fluid is defined as a material which can resist an external shear force only through motion. Newtonian fluids are those which have a constant relationship between the amount of external shear force or stress and the amount of motion or strain rate. The air we breath is such a Newtonian fluid.

Newtonian fluid motion is described by a set of equations called the Navier-Stokes equations. These equations include an expression of continuity (conservation of mass), an expression governing momentum (capturing Newton's second law $F=ma$) and an expression governing temperature (a work, energy relation). Taken together these expressions can describe fluid motion.

The expression of continuity is:

$$\frac{\partial \rho}{\partial t} + \mathbf{v} \cdot \nabla \rho + \rho \nabla \cdot \mathbf{v} = 0 \qquad (1.1)$$

Where ρ is the fluid density and $\mathbf{v}$ is the fluid velocity.

There are two primary ways of looking at this equation. One is the Eulerian view in which a volume is fixed in space and accounting is performed on the boundaries of this volume. This essentially states that the the change in material density within the volume must cancel the mass transported across the surfaces of the volume (due

7

to movement of a density gradient or expansion or compression of the material) for mass to be conserved.

The other way to view this continuity equation is to adopt a Lagrangian view and follow an ensemble of molecules through time. Here we use the material derivative $\frac{D()}{Dt}$ which refers to the same piece of material over time. The material derivative is related to the Eulerian space by the definition:

$$\frac{D()}{Dt} = \frac{\partial()}{\partial t} + (\mathbf{v} \cdot \nabla)()$$

Here we see that there is one part change with time and one part transport over space. Applying the material derivative to the continuity equation gives:

$$\frac{D\rho}{Dt} + \rho\nabla \cdot \mathbf{v} = 0$$

This says that for the same group of molecules the change of density with time and expansion of the volume occupied must cancel for mass to be conserved.

The Navier-Stokes momentum equation is essentially a unit-volume version of *ma=F*. In terms of the material derivative this can be written as:

$$\rho\frac{D\mathbf{v}}{Dt} = \Sigma F$$

Unlike analysis of rigid bodies where the individual body forces are identified and summed or a distributed force is integrated, forces in fluids are separated by type. There are a number of reasons for this. First, a rigid body, by definition, maintains its internal structure under external forces while a fluid, by definition, does not. Because of this the forces internal to the fluid must be included in any analysis since they do real work and consume energy. The second benefit to separating the fluid forces by type is that for certain fluids, or under certain conditions, some types of forces can be neglected.

In Eulerian terms and including the forces by type the momentum equation is:

$$\rho\left(\frac{\partial\mathbf{v}}{\partial t} + \mathbf{v} \cdot \nabla\mathbf{v}\right) = -\nabla p + \rho\mathbf{g} - \frac{2}{3}\nabla(\mu\nabla \cdot \mathbf{v}) + 2\nabla \cdot (\mu\mathbf{S}) \qquad (1.2)$$

The first force term $-\nabla p$ is the net pressure force per unit volume. The second term is gravitational force per unit volume (other external forces such as electrical or magnetic attraction could also be included in a similar form to the gravitational force). The last two terms represent the viscous forces due to neighboring fluid.

The symbol μ represents the viscosity (or dynamic viscosity) of a fluid. This quantity relates the shear stress to the strain rate of the fluid. These concepts can be a little abstract without an example so let us look at a simple case. If two plates of area A are separated by a layer of fluid of depth Y and the top plate is moving with a constant velocity V relative to the lower plate under an applied force F the fluid will have a velocity profile as in Figure 1.3. The shear stress on the plate will be F/A and this stress will be related to the plate velocity by $\frac{F}{A} = \mu\frac{V}{Y}$. Here the constant change in velocity versus height in the fluid gives strain rate. This is different than what would usually be taken as a strain rate in a solid which would normally be reported as a percentage change in length over a known time duration. The viscosity can also be considered a rate constant in the diffusion of momentum through a fluid.
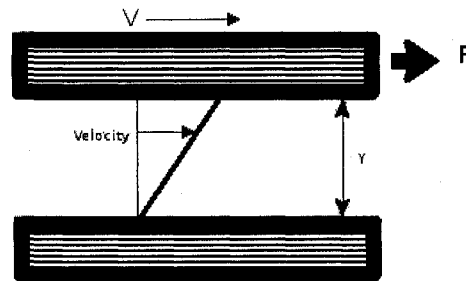
Figure 1.3: Newtonian fluid between two plates with constant relative motion.

The first of the viscous forces in Equation 1.2, $-\frac{2}{3}\nabla(\mu\nabla\cdot\mathbf{v})$, is due to gradients in the rate of expansion of a fluid. The second term, $2\nabla\cdot(\mu\mathbf{S})$ involves the strain rate tensor $\mathbf{S}$. This strain rate tensor captures the deformational motions of the fluid (or the the non-rigid body motions). These motions are those in which viscosity is important because the fluid has internal relative motion. This motion is transferred within the fluid through viscous interaction.

9

The changes of temperature within the fluid due to work performed on the fluid is expressed in the following equation:

$$\rho c_p \left(\frac{\partial T}{\partial t} + \mathbf{v} \cdot \nabla T \right) = \nabla \cdot (k \nabla T) - \frac{2}{3} \mu (\nabla \cdot \mathbf{v})^2 + 2\mu \mathbf{S} : \mathbf{S} + \beta T \frac{\mathrm{D}p}{\mathrm{D}t} \quad (1.3)$$

The left hand side represents the change in thermal energy per unit volume of the fluid. The right hand side represents various work done on, or by, the fluid. We may wonder, if we are interested only in the motion of the fluid, why must we consider the temperature of the fluid. This is largely due to the temperature dependence of the viscosity and the pressure, both of which appear in the momentum equation, Equation 1.2. For the purposes of the current work temperature will be taken as constant. The viscosity of air is fairly weakly temperature dependant in our range of interest with viscosity ranging from 1.82-1.86 Pa/s in a temperature range of 20-30°C which means there is no need to make adjustment from room temperature to body temperature.

If the flow is incompressible the Navier-Stokes equation can be simplified by removing terms involving $\nabla \cdot \mathbf{v}$ which account for the expansion of the fluid. A particular flow can be considered incompressible even if the fluid itself (such as air) is a gas. In order to consider a flow incompressible the relative change in density must be small. The density of a fluid is determined by both pressure and temperature. In our case temperature is taken as constant because of the low density of work done on the fluid. Pressure changes in our nasal models are also very small so it is reasonable to treat our flows as incompressible.

The momentum equation in the incompressible case becomes:

$$\rho \left(\frac{\partial \mathbf{v}}{\partial t} + \mathbf{v} \cdot \nabla \mathbf{v} \right) = -\nabla p + \rho \mathbf{g} + \mu \nabla \cdot (\nabla \mathbf{v})$$

Here we have taken our viscosity to be constant and move it out of the divergence operator. Both sides of the equation can then be multiplied by a problem specific scaling constant defined as $\frac{L_o}{v_o^2 \rho}$ where L_o is a length scale, v_o is a characteristic velocity in the problem and ρ is, again, our fluid density.

The momentum equation then becomes:

10

$$\frac{L_o}{v_o}\frac{\partial(\frac{\mathbf{v}}{v_o})}{\partial t} + \frac{\mathbf{v}}{v_o} \cdot L_o \nabla \frac{\mathbf{v}}{v_o} = -L_o \nabla \frac{p}{v_o^2 \rho} + \frac{g L_o}{v_o^2} + \frac{\mu}{v_o \rho L_o} L_o \nabla \cdot \left(L_o \nabla \frac{\mathbf{v}}{v_o} \right)$$

Substituting $\mathbf{v}^* = \frac{v}{v_o}$ as the non-dimensionalized velocity, $p^* = \frac{p}{v_o^2 \rho}$ as the non-dimensionalized pressure, Fr= $\frac{v_o}{\sqrt{gL_o}}$ as the Froude number and Re= $\frac{\rho L_o v_o}{\mu}$ as the Reynolds number gives:

$$\frac{L_o}{v_o}\frac{\partial \mathbf{v}^*}{\partial t} + \mathbf{v}^* \cdot L_o \nabla \mathbf{v}^* = -L_o \nabla p^* + \frac{\hat{g}}{Fr^2} + \frac{1}{Re} L_o \nabla \cdot (L_o \nabla \mathbf{v}^*)$$

If we now look at the differential operators, we would like to non-dimensionalize our physical dimensions (x,y,z) with L_o and time with $\frac{v_o}{L_o}$ giving $x^* = \frac{x}{L_o}$ and $t^* = \frac{t v_o}{L_o}$.

In the general case, if we make the variable substitution $k^* = ak$ where a is a constant $dk^* = adk$ and $a\frac{d}{dk^*} = \frac{d}{dk}$. In our case $\frac{\partial}{\partial x^*} = L_o \frac{\partial}{\partial x}$ and $\frac{\partial}{\partial t^*} = \frac{L_o}{v_o}\frac{\partial}{\partial t}$. We then have the fully non-dimensionalized momentum equation as:

$$\frac{\partial \mathbf{v}^*}{\partial t^*} + \mathbf{v}^* \cdot \nabla^* \mathbf{v}^* = -\nabla^* p^* + \hat{g} Fr^{-2} + \frac{1}{Re}\nabla^* \cdot (\nabla^* \mathbf{v}^*) \qquad (1.4)$$

Note that if the Re number is large the viscous term is eliminated while if the Fr number is large the gravitational term is eliminated.

It is common in fluid mechanics to employ non-dimensionalized numbers which capture important ratios of the problem at hand. These non-dimensionalized numbers provide some abstraction from the unit system used but more importantly are transferable across similar problems at different scales. For instance a non-dimensionalized number which includes the dimensions of the problem has the same meaning for many scales of the same geometry. One such common non-dimenionalized number is the Reynolds number which looks at the ratio of the convective terms and viscous term and includes a length scale from the geometry containing the flow. This means a Reynolds number of 10 based on diameter has a similar meaning for a tiny tube or a large pipe and for fluids of low or high viscosity or density, respectively.

The Reynolds number is important because it compares the kinetic energy per unit volume in the flow with the shear stress which tends to dissipate energy in the flow and reduce momentum though viscous losses.

11

Flows of gases with suspended aerosol particles are also well described by the Navier-Stokes equations as long as the concentration of the aerosol particles are not too large. If the concentration of the aerosol becomes high enough the effect of the particle inertia and drag on the flow must be considered.

In the current work we are mainly interested in aerosol deposition by inertial impaction. That is, by aerosol particles striking surfaces where the gas flow changes direction. The two other main causes of aerosol deposition are gravitational settling, which is important for large particles in relatively still conditions, and diffusional deposition, which is important for very small particles.

In considering inertial impaction two non-dimensionalized numbers are important to understand. The Reynolds number, already discussed, is defined for our purposes as:

$$\mathrm{Re} = \frac{\bar{Q}\rho}{D\mu}$$

where:

- D is a length scale

- $\bar{Q}$ is the average volumetric flow rate

- ρ is the fluid density

- μ is the fluid viscosity

By comparison with our previous definition of the Reynolds number we see that the characteristic velocity is taken as $\bar{Q}/D^2$.

The Reynolds number is the main non-dimensionalized number used to characterize incompressible flows. The other number which can be important is the Froude number which compares kinetic energy per unit volume to the work of gravity. In our case gravity is not an important factor compared to the kinetic energy and can be ignored.

The other non-dimensionalized number of importance in inertial impaction is the particle Stokes number which is defined as:

$$\text{Stk} = \frac{\bar{Q}\rho_{particle}d^2 Cc}{18\mu D^3}$$

where:

- $\bar{Q}$ is the average volumetric flow rate

- $\rho_{particle}$ is the particle density

- d is the particle diameter

- D is the length scale

- μ is the fluid viscosity

- $Cc = 1 + 2.52\lambda/d$ is the Cunningham slip factor

- λ is the fluid molecular mean free path

An object which has velocity relative to a surrounding fluid will experience drag. Flows of low velocity or of high viscosity fluid have low Reynolds number and are called creeping or Stokes flows. For Reynolds numbers less than about 0.5 the expression known as Stokes law gives the drag force on a sphere as:

$$F_D = 3\pi\mu dU$$

where:

- U is the relative sphere/fluid velocity

- d is the sphere diameter

- μ is the fluid viscosity

The mass of this sphere is given by:

$$M = \frac{\rho_{particle}\pi d^3}{6}$$

Using Newton's second law (F=ma) with the drag force acting opposite the direction of travel we can look at the acceleration caused by the fluid drag on the sphere.

$$-3\pi\mu\frac{dx}{dt} = \frac{1}{6}\rho_{particle}\pi d^3\frac{d^2x}{dt^2}$$

Simplifying and substituting $v = \frac{dx}{dt}$ gives:

$$v = -\frac{d^2\rho_{particle}}{18\mu}\frac{dv}{dt}$$

this has the form

$$v = a\frac{dv}{dt}$$

separating variables and integrating once gives

$$v_o e^{\frac{t-t_o}{a}} = v = \frac{dx}{dt}$$

setting t_o to 0 and integrating again

$$a * v_o\left(e^{\frac{t_f}{a}} - e^{\frac{t_o}{a}}\right) = x_f - x_o$$

taking t_o and x_o as zero and letting t_f become large (a is negative)

$$a * v_o(-1) = x_f$$

$$\frac{v_o d^2\rho_{particle}}{18\mu} = x_f$$

By comparison of the the definition of the Stokes number to the definition we have derived for the stopping distance, x_f, we find:

$$\text{Stk} = \frac{v_o d^2\rho_{particle}}{18\mu D} = \frac{x_f}{D}$$

The Stokes number is probably best understood as relating the stopping distance of a particle in a fluid flow to a characteristic dimension in the geometry containing the flow. This indicates a particle's ability to follow curves in the flow pattern or stream lines. The larger the Stokes number the greater the deviation will be between particle paths and curved streamlines relative to the scale of the containing geometry.

The particle aerodynamic diameter, which is an often quoted property of an aerosol particle, is the diameter of a droplet of water that would behave like the particle of interest. It is defined as:

14

$$d_{ae} = \sqrt{sg}d$$

where:

- sg is the specific gravity of the particle of interest

- d is the diameter of the particle of interest

This identity is generated by equating the settling velocity based on the Stokes drag of a particle of unit specific gravity and of the aerodynamic diameter to that of the particle of interest and solving for the aerodynamic diameter. This aerodynamic diameter combines the particle diameter and particle density in a way that normalize it to a water droplet.

A metric that is often used when discussing aerosol deposition by inertial impaction is the impaction parameter which is equal to $d_{ae}^2 Q$ where d_{ae} is aerodynamic diameter. This is a dimensional quantity but it is clear that it is proportional to Stokes number for constant particle density, geometry and fluid.

Further background related to aerosol deposition can be found in Finlay[12].

1.4 Experimental Work

There have been a number of *in vitro* and *in vivo* studies of nasal deposition. For example *in vivo* adult studies have been performed by Heyder et al., [15], Cheng[5] and Rasmussen et al.[38]. A review of a number of these studies in both the impaction and diffusional regimes is given by Cheng [5]. Of particular interest are studies by Bennett [2] and Becquemin [1] which make *in vivo* measurements of nasal deposition in children and adults during varying levels of activity. They find that nasal deposition is significantly less for children than adults in similar activity states.

Some *in vivo* studies have been performed to investigate lung delivery of aerosols from pressurized metered dose inhalers with spacers [45, 46]. These studies do not capture the filtration efficiency of the nasal airway but compare lung dose to delivered dose over the size range produced by the inhaler.

A number of *in vitro* studies have been performed using nasal replicas of adults [27, 4]. Monkey airway replicas have also been used for comparative studies [28]. Models of infant airways have been constructed by several authors [44, 21, 6]. The SAINT infant replica is discussed in greater detail in Section 1.5. Models were created by Cheng et al. based on magnetic resonance imaging (MRI). These models included a 1.5 year old, 2.5 year old and 4 year old and were used to measure deposition of particles in a size range of 0.008 to 0.03 µm where diffusional deposition dominates[6]. Swift generated a model of a 6 week old infant girl based on magnetic resonance images. Coronal sections of 3 mm thickness matching the magnetic resonance imaging slice thickness were hand carved in plastic and assembled to form the model. Experiments where then performed to characterize the nasal filtration function of this model in the impaction range. These involved salt particles whose concentration was measured upstream and downstream of the model under constant flow rate conditions[44].

1.5 SAINT Model

A copy of the model described by Janssens et al.[21] was obtained through Erasmus MC, Rotterdam, Netherlands and was included in the set of replicas used for this study. This model was constructed based on a CT scan of a 9 month old girl performed to capture an isolated skull defect. The model was built in a photo sensitive resin using a laser print head.

The model was validated by comparing CT images of the constructed model to the original CT images of the subject and found to be in good agreement.

Experiments performed with this model are numerous and include:

- Size characterization by an Andersen cascade impactor of budesonide delivered from a pMDI through a spacer[21].

- Pressure drop measurements versus constant flow[21].

- Measurements of simulated lung dose using breathing patterns captured from sleeping and awake infants to estimate the effectiveness of providing aerosol

therapy when infants are sleeping[25].

- Comparisons made of simulated lung dose for inhalers which employ HFA propellants versus those that use CFC propellants[23].

- Exploration of the effect of breathing rate and tidal volume on inhaler output and simulated lung dose delivered by various inhalers[24].

- A study looking at the mass median aerodynamic diameter of the simulated lung doses from a single nebulizer under different tidal volumes and breathing flow rates[42].

- A study examining the effect of the position and size of face mask leaks on inhaler output and simulated lung dose[11].

It was desirable to include this model in the set of models examined since it is familiar to people from such previous work. It is also an independently validated model which provides a useful point of comparison for the models constructed by us for this project.

1.6 Accounting for Inter-subject Variability in Infant Nasal Deposition

The goal of this project was to develop a predictive model for total deposition by inertial impaction in the nasal airways of the very young. To be effective this model would have to account for inter-subject variability through a dependence on the nasal geometry of the individual. Otherwise the uncertainty in predicted deposition due to differences from individual to individual was expected to be very large. In order to determine the appropriate dimension, or dimensions, to use, a sufficient population was studied so that different dimensions could be tried and the ones which best accounted for the experimental data across the whole group could be found.

17

Based on the facilities available and the scope of the project, *in vivo* work was not possible. Instead *in vitro* experiments using nasal airway models along the lines of those performed by Grgic[14] for the oral airway were planned.

There were three main efforts involved in this project. The first was to obtain the required medical scans and construct the infant nasal models. The second was to develop an experimental procedure and collect deposition data for a range of particle sizes and breathing patterns for each model. The third was to develop a predictive model which accounted for the observed data in all individuals.

An accurate method to predict individual nasal deposition allows individual, quantitative estimation of lung dose for an infant receiving aerosol pharmaceuticals. It also provides a measure of nasal filtration of hazardous environmental aerosols on an individual basis.

If the geometric parameter which is used to account for inter-subject variability is known for individuals in a population, the statistics could be calculated on the filtration curves for that population. For instance the average filtration could be found for the group or the filtration at plus one standard deviation could be calculated. This could provide valuable guidance for safe exposure levels to hazards and also general dosage guidelines for pharmaceuticals. In this way we hope to replace the difficult task of measuring aerosol deposition with the somewhat easier task of measuring airway geometry.

If the geometric parameter which is used to account for inter-subject variability is not available, mean deposition for the group we have studied can still be used for prediction of nasal filtration, though the individual may fall fairly far from this average curve.

1.7   Empirical Correlations

Empirical studies have been directed towards understanding the variables that control nasal deposition so that it can be predicted in the individual. Many correlations have been explored. An early study by Hounam et al. [17] correlated nasal deposition with nasal resistance or pressure drop during flow. More recent work [5, 44, 27]

18

has focussed on the Stokes number as the key parameter determining nasal deposition.

The Stokes number is a natural parameter of interest as it relates the stopping distance of a particle in a flow to the dimensions of the airway. A key question is which airway dimension should be used to define the Stokes number. The minimum cross sectional area of the airway has been the parameter of choice [5, 44, 27] as it seems to provide a good collapse of the inter-subject data in adults.

Since the nasal geometry is complex and changes dramatically along the path the aerosol particles must follow to exit the nose, it is not obvious that a single geometric parameter can be used to describe it. Part of the appeal of using minimum cross sectional area in the Stokes number is that it corresponds to an area of high regional deposition in the adult nose. A study by Itoh et al.[20] looked at regional deposition for particles of varying size and observed high deposition for particles of 1.3 μm aerodynamic diameter just posterior to the minimum cross section. Larger particles of 4 μm deposited mainly at the anterior end of the middle turbinate. Itoh attributed this to smaller particles being transported by turbulent diffusion in the expansion region just past the nasal valve while larger particles have too great an inertia to be transported in this way and instead impact on the turbinates where the flow changes direction from an upwards path to a horizontal direction following the turbinates.

The expansion of the flow as it emerges from the nasal valve is thought to introduce turbulent eddies. The usage of actual values of the minimum cross-sectional area, A_{min}, seem to be somewhat confused. Cheng[5] quotes an average value of A_{min} based on MRI of 10 subjects as 208 mm^2, Lang[32] gives a value of 20-60 mm^2 while Itoh et al.[20] give a diameter of 2.2 mm corresponding to a total area of 30.4 mm^2. Clearly the numbers of Cheng seem to differ greatly and perhaps there is an important change from the live state to the cadaver.

Most adult studies and a study by Swift [44] of a child replica do not show any flow rate dependence on deposition that is not captured by Stokes number. The study by Itoh et al.[20] does show Reynolds dependence in an adult model through

19

use of carrier gasses of different densities.

1.8 Extension to Prior Art

The author is not aware of any *in vivo* data on nasal deposition by impaction for the ages studied. The model constructed by Swift [44] of a 6 week old female infant was used to collect particle impaction data but the flow rates used were 5 L/min to 20 L/min. These are quite high flow rates for an infant of this age. The maximum flow rate considered in the present study is 11 L/min for children of older age. A girl of 6 weeks would on average weigh 4.4 kg and have a resting tidal volume of approximately 26 ml[7] and a breathing rate of 48 breaths per minute [10]. This would suggest a resting flow rate of 2.5 L/min.

Models constructed by Cheng [6] of a 1.5 year old, a 2.5 year old and a 4 year old were used in deposition studies in the ultra-fine particle size range 0.0046 to 0.2 μm. These particles deposit through diffusion rather than impaction.

There have been a number of studies based on the Saint replica [21]. Most of these have looked at inhalers or other polydisperse sources without trying to map the filtering function of this model. A number of these papers are discussed in Section 1.5.

The current work involves 11 subjects which is a much larger set than considered previously. This is a large enough number of individuals to try to account for inter-subject variability in nasal filtration. This has not been attempted in infants to date and would provide a method to predict aerosol deposition in the individual infant. The dependence of deposition on breathing pattern will also be made more clear which is useful when considering alternate methods of aerosol therapy such as administering medications during sleep [25].

1.9 Study Methods

Models were generated from source computed tomography data using various commercial computer aided design tools created for medical modeling. Models were

built in acrylic plastic using a rapid proto-typing machine. The models included the nasal airway from the nostrils to just past the larynx and a large section of the face surrounding the nose.

The plastic models were connected to a breathing simulator so that air could be passed through the models in a realistic, periodic fashion. Aerosol composed of a wide size range of oil droplets was introduced into a chamber containing the model. The amount of aerosol that passed through the model was compared to the amount of aerosol that passed through a sample line for several distinct size ranges. In this way it was possible to measure the amount of filtration caused by the model at different particle sizes and breathing rates.

Both the geometry of the nasal airway and the amount of deposition for a given particle size and flow rate varies greatly from individual to individual. In order to predict nasal deposition in an individual the source of this variation in deposition must be correlated to the changes in nasal geometry. For this reason a collection of 11 different airways were examined in this study in order to try to find a common trait that could used to predict deposition. Different correlations where examined in order to best relate the individual geometry to the rates of deposition.

Chapter 2

Nasal Replicas

2.1 Model Construction

The current project required the construction of a number of models of nasal airways in order to examine the causes of inter-subject variability in infant aerosol deposition. A portion of the face around the nostrils was included in the models in order to have a realistic entrance condition for the flow (and for possible future experimentation with face-masks). It was desired to work with as young a group of subjects as possible since much of the existing work had been performed in adults and the greatest new understanding would be gained by looking at the very young. In addition, the nasal route for pharmaceutical aerosol delivery is of primary importance for the very young as older children and adults typically use oral delivery devices.

With the approval of the Alberta Health Research Ethics Board and through the generosity of Dr. Michelle Noga in radiology at the University Hospital we were able to obtain a number of cranial computed tomography (CT) scans of infants. Ten of the scans obtained of infants aged three to 18 months were suitable for our nasal modeling. In general those scans that were discarded did not extend far enough down the neck of the subject to include the larynx. All scans were obtained with the patient in the supine position. Imaging was helical with reconstructed axial slices of 1.25 mm thickness and in plane resolution ranging from 291 μm to 430 μm across subjects.

These infants had undergone scanning for unrelated skull conditions or head trauma and were deemed to have normal airways. The re-use of this existing data was by far the best possible way to obtain the required imagining. There was no possibility of performing CT scans for the purposes of this research study since the scan represents a significant radiation dose in very young subjects and would not be ethical for this purpose.

The other option considered was to add an additional sequence onto MRI scans that were scheduled in infants for other diagnostic purposes. This had its own associated risks since these very young patients would be scanned under anaesthetic and extending the duration of the scan increases the potential for complications related to the anaesthetic. Additionally, based on our experience with adult MRI scans of the nasal airway, there may have been some difficulty in obtaining the resolution and contrast needed to accurately model the infant nasal passages. Partitioning of the airway from the rest of the MRI data is also a more difficult and subjective process than partitioning of CT data.

In order to translate the source CT data into an airway model the airway must be identified and separated from the rest of the CT data. This process is often called partitioning since the CT data is being divided based on anatomical divisions into different parts.

The airway was partitioned from the CT based on grey-scale value thresholding. Unlike MRI data a single thresholding of the CT data within a single subject provided a very consistent partitioning. Threshold levels were adjusted from subject to subject based on inspection of several coronal slices (slices parallel to the plane of the face). A coronal slice showing the airway partitioning in subject 7 is shown in Figure 2.1 where the light shading is the airway. The faces of the infants were partitioned using thresholding and by manually selecting regions within the face including the airway in order to create a solid face volume. CT data import and partitioning work was performed in Mimics versions 9 and 10.11 (Materialise, Ann Arbor, MI) at the medical modeling laboratory of COMPRU.

Most of the infants had breathing tubes in the nares during CT scanning which
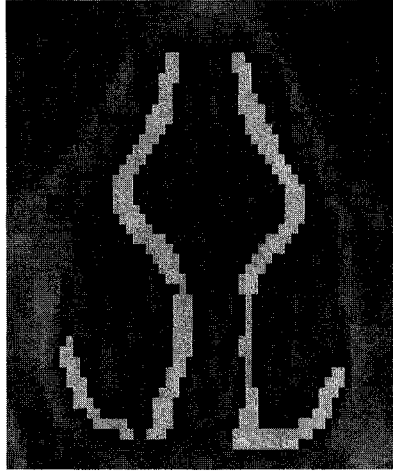
Figure 2.1: Airway partitioning in patient CT data.

had grey-scale very similar to that of the facial skin. These breathing tubes were manually separated from the face by pixel selection in multiple planes. In general the nostrils were an area which caused particular difficulty in partioning and modeling. Since the outside of the face is surrounded by air, thresholding will not limit the airway at the nares and the extend of the airway must be manually limited at the nostrils. The partitioned airway and face were converted to 3D volumes and exported from Mimics in stereo lithography (STL) format.

Smoothing was then performed on the face and airway using Magics version 9 (Materialise). Newer versions of Magics have a much less aggressive smoothing algorithm which was not found to be very effective. The airway was smoothed in two stages. First the airway was smoothed at 25 iterations, a characteristic metric was calculated, in this case surface area divided by volume, and the smoothing was undone to return the airway to its original state. This metric was characteristic of the basic smoothed shape of the airway and approached a limiting value exponentially with smoothing iteration. Figure 2.2 shows the changes of the characteristic metric with smoothing iteration for a pair of adult nasal airways to demonstrate the method. Smoothing was again performed until a certain percentage of the limiting value was achieved. The same percentage was used for all airways to produce a consistent

24

level of smoothing. This smoothing method bears some similarity to the roughness measure proposed by Lavoue[33] and is a method to normalize the smoothing to the airway shape so that a consistent level of smoothing can be achieved across multiple subjects. The face was smoothed in a more subjective manner and local smoothing was applied to areas of roughness where the oxygen tubes had been removed from the imaging data. After smoothing the models were saved as STL and imported into Magics version 11 for additional processing.
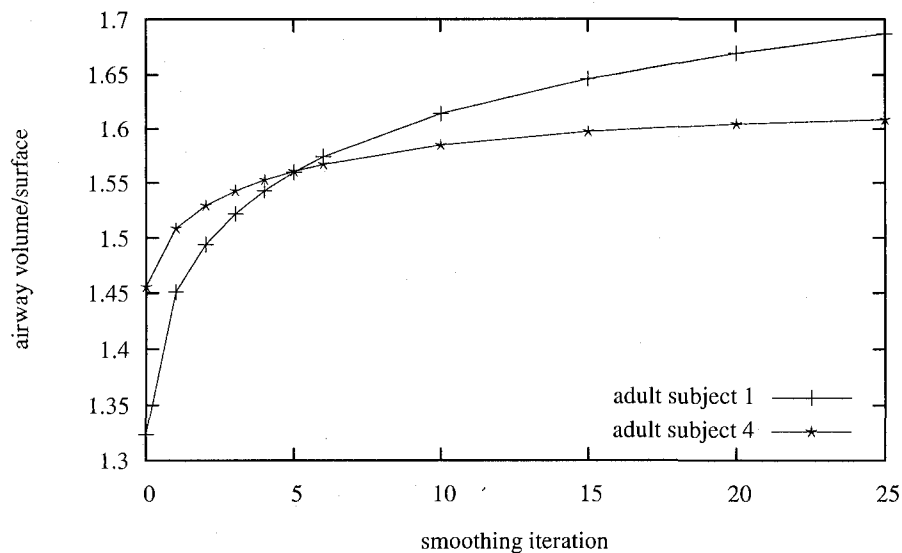
Figure 2.2: Characteristic metric versus smoothing iteration

The solid representing the face was augmented with additional solid geometry in order to contain the airway posterior to the face to beyond the larynx. This was done by joining the face with simple geometries like cylinders. The outlet of the model was formed by a cylinder 15 mm in diameter and approximately 20 mm in length. This was the interface to the 15 mm inside diameter tubing used to draw air through the model and was a size that conveniently contained the airway in all cases. The airway itself was extended for approximately 20 mm using a cross-section just distal to the larynx in order to form an exit of constant cross-section.

The solid geometry that was to contain the airway was then separated into two

25

portions at a convenient point distal to the nasal pharynx. The airway was then subtracted from the two solids which would contain the airspace. The extents of the face and the airway were chosen so that the region around the nostril entrance was defined by the airway rather than the face ie. the nostril was solid in the face. Because smoothing was performed on the airway and face separately there was often a slight ridge along the nostril where the subtraction was performed. This area was again smoothed with a local smoothing in Magics version 9 to remove any roughness at the entrance.

The models were then submitted in batches to the rapid proto-typing machine (Invision SR 3-D printer from 3D Systems, Rock Hill, SC). The models were built with acrylic plastic (trade name VisiJet SR 200) with a wax support material (trade name VisiJet S100). When complete the models were removed from the build platform and placed in an oven at $65°C$ to melt the wax support. This heating was repeated several times with washing in hot water after heating to flush the wax out of the interior of the model as well as possible. The wax support material offered a number of advantages over other available support systems which employed either narrow rigid struts of the build material or a hard support material distinct from the build material. A hard support material would be much more difficult than wax to remove from the narrow airways while hard struts would leave a rough base where they were snapped out of the geometry.

The two parts of the models were connected using lengths of threaded rod and seams where the two parts of the models met were joined on the outside with putty to prevent any airflow through the seam.

Pictures of the constructed model of subject 10 are shown in Figure 2.3. The two components of this particular model are joined with vertical nylon thread stock. Figure 2.4 shows the assembled model of subject 7. In this case horizontal nylon thread stock joins the throat portion of the assembly to nuts glued into the recesses in the model face. Sealing putty can be seen in the images for both subjects.

After the experiments were performed the models were CT scanned and dimensions were compared with the dimensions sent to the rapid proto-typer. Slight
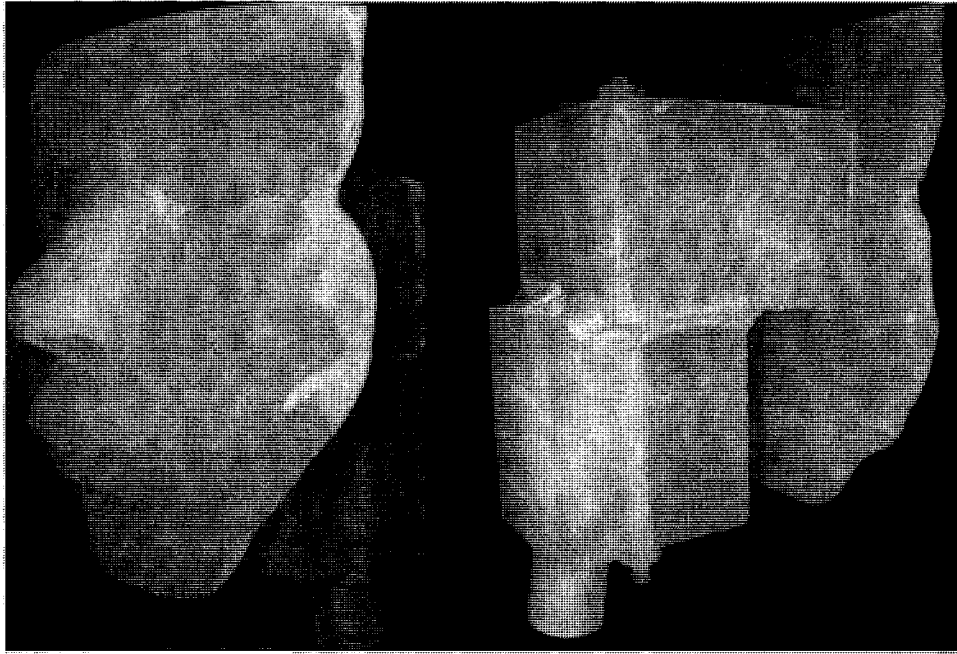
Figure 2.3: Assembled model of Subject 10, front and back views.
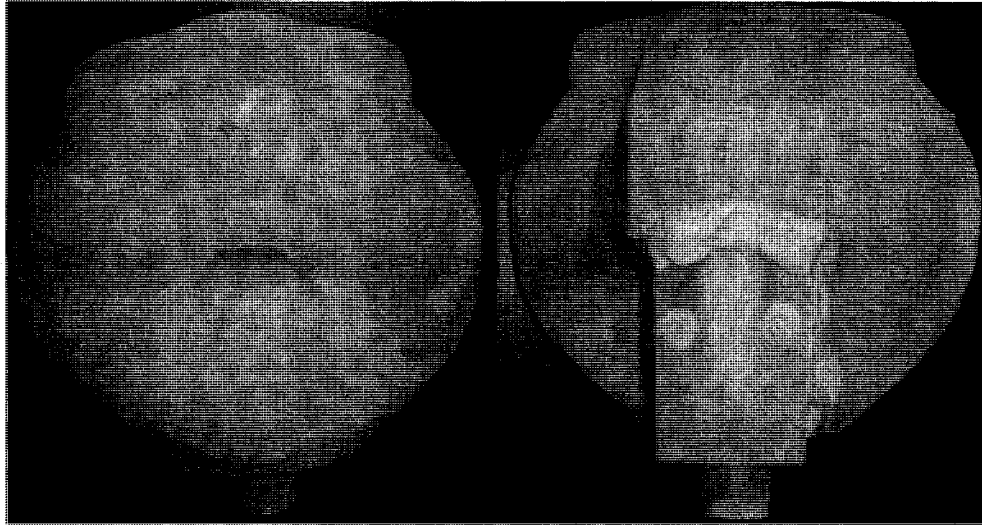
Figure 2.4: Assembled model of Subject 7, front and back views.

differences in the critical metric (vol/surface area) were found but these differences

27

where much less than the inter-subject variability of this metric. A number of dimensions as defined in Table 2.1 were compared before and after building the models in order to quantify the differences in the pre-build and post-build STL files. Volume differed on average by 5.28%, airway surface by 5.24%, minimum cross-sectional area by 3.93%, the computed parameter D differed by 7.85% (tending to be larger in the models than the original CT data), while length remained unchanged. Visually the model airway was a very good match to the original scanned airway as can be seen in Figure 2.5. In addition the alignment of the two parts making up the model assembly seemed to be quite good for all models.

The full set of nasal airways used in this project, ordered by age, is shown in Figures 2.6 and Figure 2.7 which shows the opposite profile. These images are based on CT scans of the completed models and clearly show the large differences in nasal geometry between subjects.

2.2   Measuring Model Dimensions

All models used were CT scanned in order to determine the actual airway dimensions with which the experiments were performed. The airway was partitioned from this CT data based on grey-scale value. The same threshold was used to identify the airway in all models built in acrylic while a different threshold was used for the SAINT model which was built using a different plastic. The STL file generated from this partitioning was imported into the Rhinoceros (McNeel, Seattle, WA) modeling tool and the pertinent dimensions were measured using features in that tool. The minimum cross-sectional area was found by inspecting the airway and choosing a location which appeared to be the minimum cross section. Cross-sections upstream and downstream where tried for one subject to confirm the method.

The dimensions of the models and the age and genders of the subjects are given in Table 2.1.
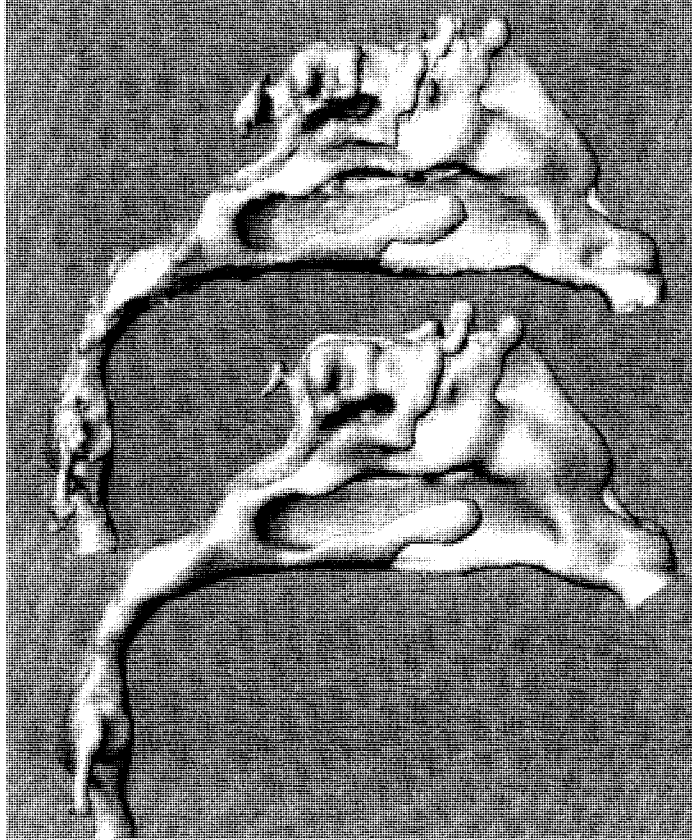
Figure 2.5: Comparison of planned airway and built airway. Top is airway as extracted from the original CT. Bottom is airway extracted from built model.

2.3 Roughness and Detail

The issue of roughness in the infant nasal model is complicated by the fact that the geometry itself is small and naturally convoluted. Based on photos of nasal tissue in Lang[32] and the fact that the interior of the nose is known to be covered by a layer of mucus a high level of surface smoothness is to be desired in the nasal models.

There are a number of steps in the modeling process and each can be considered a kind of transform that can effect both roughness and level of detail. These steps are outlined below with some comments on their likely effect:

- The process of CT scanning the patient introduces a discretization of what is
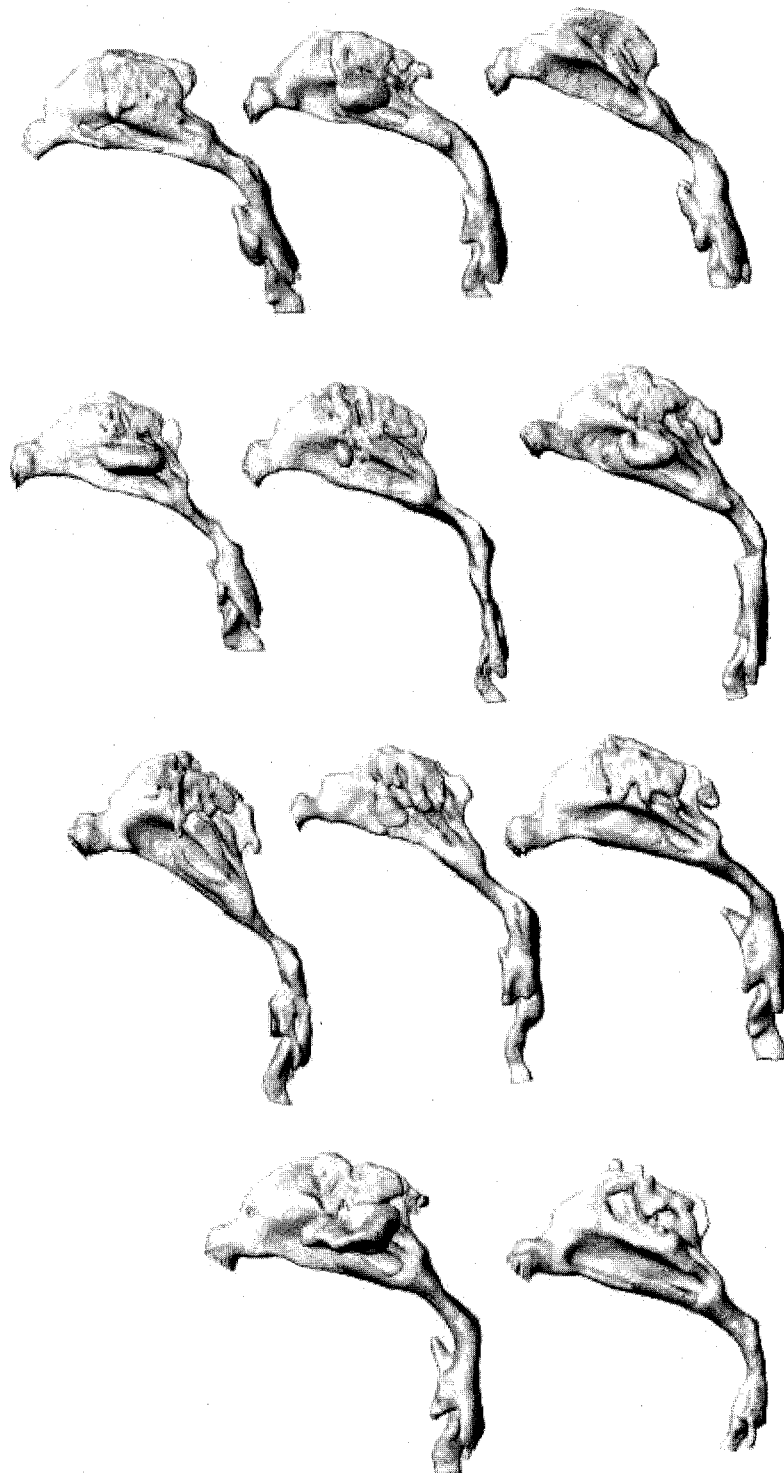
Figure 2.6: Left side of nasal airways in order of age from top left.
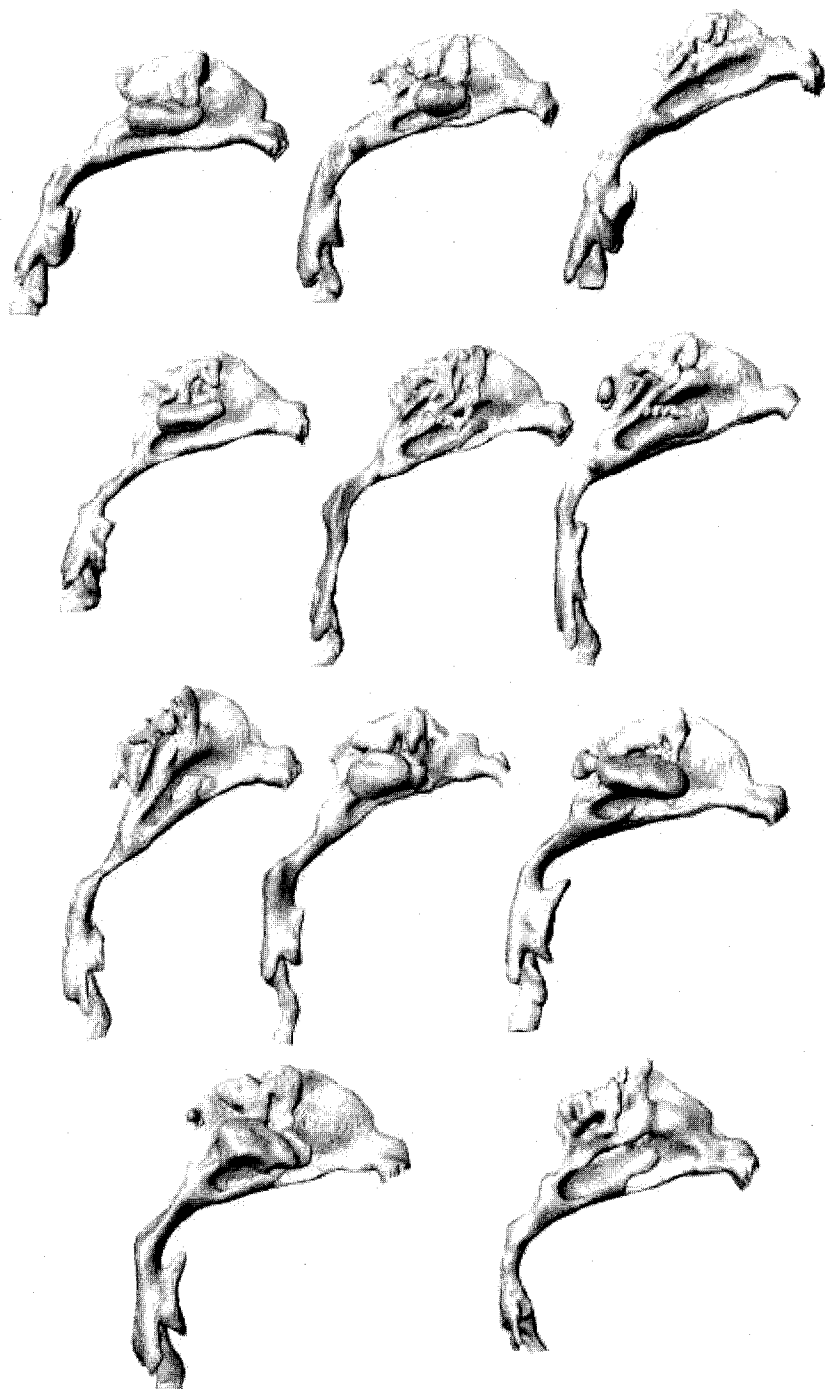
Figure 2.7: Right side of nasal airways in order of age from top left.

Sub	Age (M)	Sex	V $(_{mm^3})$	As $(_{mm^2})$	L $(_{mm})$	A_{min} $(_{mm^2})$	D $(_{mm})$
SAINT	9	F	8034	7154	113.4	31.8	1.12
2	3	M	13430	8723	95.6	65.2	1.54
3	3	M	11924	8646	100.6	64.9	1.38
4	4	F	7913	6760	98.0	45.1	1.17
5	5	F	8599	7573	89.9	66.6	1.14
6	6	M	8723	9641	110.3	58.7	0.905
7	7	M	11789	10241	109.7	54.2	1.15
8	8	M	10342	10142	110.0	73.5	1.02
10	16	M	18583	13693	111.3	62.3	1.36
11	18	F	10754	9700	100.6	84.1	1.11
14	15	M	14304	11331	115.3	47.9	1.26

Table 2.1: Subject Parameters: V is volume of airway, As is the surface area of airway lumen, L is a representative path length through the model, A_{min} is the minimum cross sectional airway taken perpendicular to expected airflow, D is the calculated dimension V/As

a continuous geometry down to the cellular level. The resolution used was quite fine so this effect is reduced but this does introduce a kind of roughness on the scale of the CT voxels and limits the feature detail to several voxels. This is an important factor in our models since some air passages are only one or two voxels wide. Beyond discretization there will always be noise in real data. Since the signal in CT is generated by X-rays which are harmful to the individual being scanned the signal to noise ratio in the the resulting data is likely carefully managed with the patient well being in mind.

- Image segmenting or partitioning is performed. In this case thresholding was performed which is quite consistent throughout the model. Again this works on single voxels. Partial voluming will occur in the CT data where individual voxels straddle the air tissue interface and these voxels will be assigned an intermediate grey-scale value. This partial voluming is part of the discretization of the CT process and will be reflected in the partitioned data. After the voxels of interest are selected they are converted into a stereo lithography (STL) format. This format captures complex surfaces using a set of small triangles with shared vertices. This conversion has some smoothing effect since the

square volumes of the voxels are replaced by smaller, more flexible surfaces.

- The models are then smoothed using a smoothing algorithm. The details of the algorithm are not known since it is a built-in feature of the Magics software. Some smoothing algorithms operate by "curvature flow" which essentially uses a diffusion operator to diffuse local curvature over the surface based on a curvature gradient[8]. By running many iterations of smoothing the effect is exaggerated and it can be seen that fine detail is lost while the coarse features of the model are preserved. There is also some volume reduction associated with the Magics smoothing algorithm even when shrinkage compensation is enabled. The desired effect of smoothing is to remove roughness and noise while maintaining all actual features. Unfortunately there is no perfect way of distinguishing between the noise and actual features. Normally, small features are removed while larger features are maintained. In our case smoothing reduced unwanted roughness with little reduction in detail.

- The build process has its own effect on detail and roughness. The claimed resolution of the printer used is 42 μm in the Z direction and 77 μm in X,Y directions. In general the print quality seemed to be very good and little detail was likely lost. Since the surfaces of interest inside the nasal airways were not generally aligned with any of the build planes some roughness would be introduced by the discrete resolution of the printer.

- The removal of the wax support material was likely responsible for a measurable loss of detail and introduction of surface roughness. The wax was melted and models were repeatedly rinsed in hot water to remove the wax support from the internal geometry. Even after this process there is still a waxy residue on the interior surface of the models and it is likely that wax in very narrow openings may remain due to high surface tension in these structures. This wax would smooth in some areas while introducing some roughness in others and almost certainly reduces some fine detail in the airway.

CT scans of the final models were performed with a resolution of 234 μm for the SAINT and subject 11 and 430 μm for all others. This is quite suitable for comparing the structure of the final model to that of the original scan but is not suitable for capturing surface roughness.

The effects of roughness in narrow channels is still a topic of research as discussed by Kandlikar et al.[26]. One of their topics of interest is the effect of roughness features that are greater than 5% of the channel dimension. This may be pertinent in the case of our models since some of the channels are on the order of 1 mm/1000 μm, 5% of which would be 50 μm which is slightly finer than the claimed resolution of the rapid proto-typing hardware. Kandlikar et al. are able to well predict the drag co-efficient at laminar flow velocities by calculating a reduced dimension of the available flow cross-section due to an effective narrowing caused by the surface roughness in the channel. They are not able to predict well the drag co-efficient in the turbulent flow regime but did notice an earlier onset of turbulence in narrower channels of the same roughness.

On the basis of personal communications with my colleague, Laleh Golshahi, who performed some preliminary deposition measurements on MRI based adult nasal models built with and without smoothing using the same build system used for the infant models, it would seem that the effect of software smoothing on deposition is less than the intersubject variability in deposition for adults.

It is not obvious what level of detail needs to be maintained in a nasal model to accurately capture aerosol deposition. The nasal airway could be considered a set of parallel paths with a common pressure drop. The flow will tend to be greater in the paths of larger calibre and most of the aerosol transport will occur there. However the deposition may occur preferentially in the narrow paths and the fine detail may have a significant effect even on the flow pattern in the larger spaces.

Some ideas for experiments are mentioned in Section 5.4 to better understand the issues of roughness and fine detail.

The SAINT model was built by a separate group using a different rapid proto-typing method and a different material. Despite the differences in generation and

construction of the SAINT model it follows the trends of the other models very closely suggesting that if roughness is an important factor it must be having a similar effect across modeling methods.

Chapter 3

Deposition Measurement

3.1 Experimental Setup

The objective of the experiments performed was to characterize the filtration of aerosol of different sizes in the infant nasal replicas under various, physiologically realistic, breathing conditions.

The experimental setup used is depicted in Figure 3.1.
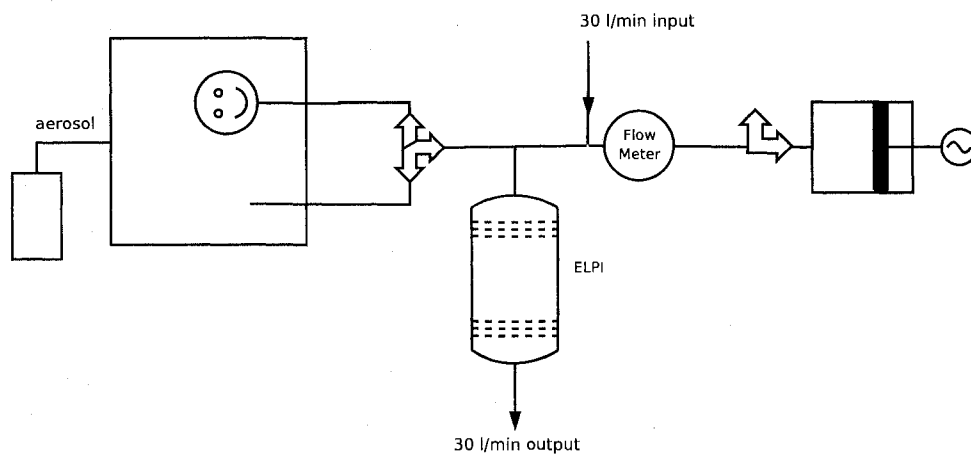
Figure 3.1: Experimental Setup

From upstream to downstream the setup consisted of the following:

- A 6 jet collison nebulizer (BGI, Inc. Waltham, MA) connected to filtered house air producing a polydisperse aerosol of sunflower oil (ρ=0.92 g/ml).

36

- A chamber, equipped with a mixing fan, housing the airway model and a blank sampling line of matched length.

- A three way valve to switch between the model and the blank sampling line.

- An electronic low pressure impactor (ELPI) (Dekati Ltd., Tampere, Finland).

- Filtered air-supply matched to the flow volume through the ELPI.

- A mass flow meter (4143 series, TSI) measuring breathing pattern.

- One-way valve attached to the breathing machine allowing only inhalation flow through the airway model.

- Cyclic, syringe type, breathing machine, constructed in-house, producing sine wave breathing patterns.

A photo depicting a representative arrangement of the apparatus used is shown in Figure 3.2. The ELPI, mixing chamber, mixing fan, model, sampling line can be seen in this photo. It is also possible to see a part of the collison nebulizer through the mixing chamber.

Deposition was measured by comparing the amount of aerosol that passed through the blank sample line to the amount that passed through the nasal model under similar flow conditions. No separate characterization of aerosol inhalability was performed and all measurements of deposition indicate the full fraction that did not pass through the model. Aerosol entered the replica naturally from the air surrounding the facial features of the replicas, so that the present results include both inhalability effects and internal nasal deposition. Inhalability is thought to be close to 100% for the flow-rates and particle sizes considered here based on results by Kennedy[29].

The ELPI is the primary measurement instrument in this experiment. In the physical configuration of the ELPI as used, the device included a cascade impactor consisting of 13 stages the bottom twelve of which were connected electrically to a multi-channel electrometer. It is a low pressure impactor because the bottom stages

37
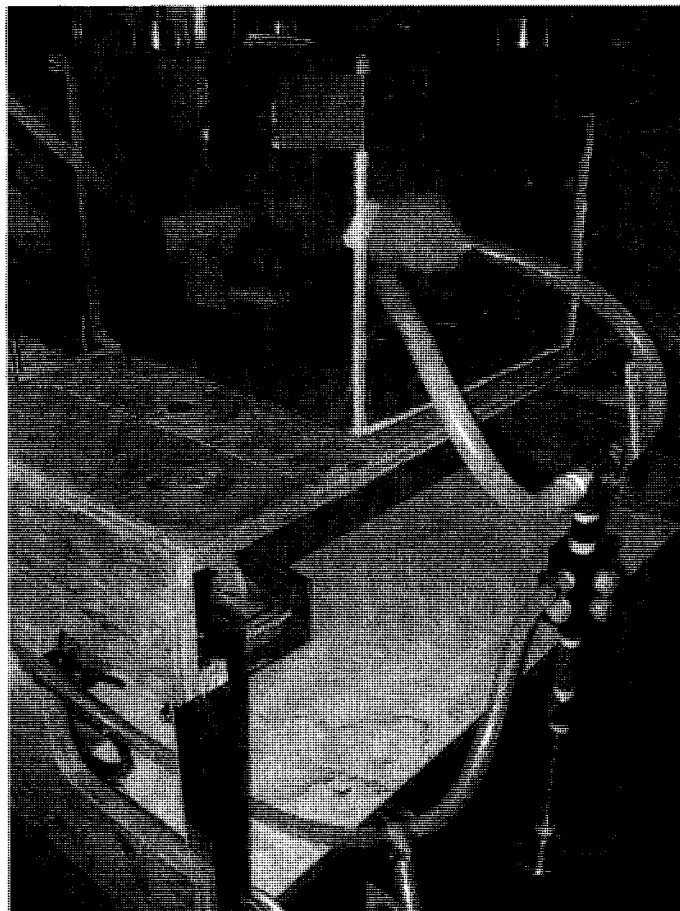
Figure 3.2: Photo showing measurement chamber.

are operated at below atmospheric pressure. A corona charger is situated upstream of the impactor in the instrument. The corona charger introduces charge to the passing aerosol particles. The particles then impact on one of the 13 collection plates in the impactor based on their aerodynamic diameter. The impaction of each particle transfers a charge to the collector stage which is connected to a electrometer. The current caused by the particle impact on the collection plate is measured and converted into particle counts. Corrections are made in the system software for particles which deposit on higher stages than they ought due to diffusion. Corrections are also made for size specific losses of larger particles in the charger. The integration of the particle charger into the ELPI allows the unit to work accurately with

38

mildly charged aerosol particles since an equilibrium charge is introduced by the corona charger. This removes the need for a neutralizer in the current experimental setup.

Each jet plate, collector plate pair which forms a stage in the impactor has a cut size or D_{50} value for which 50% of the particles of that size are retained on that collector plate. The filtration curve for each impactor stage is very steep so almost all particles greater than the D_{50} size are retained on the collector plate while almost all those smaller pass on to the subsequent plates. A lower size limit is defined by the current stage while an upper size limit is given by the proceeding stage. For this reason the first stage is not connected to the electrometer since there is no distinct upper limit for particles collected on this stage. The calibrated D_{50} values in µm, for particles of unit density are given in Table 3.1.

Stage	1	2	3	4	5	6	7
D_{50}	0.028	0.051	0.088	0.151	0.259	0.380	0.610
Stage	8	9	10	11	12	13	
D_{50}	0.943	1.590	2.377	3.972	6.550	9.892	

Table 3.1: D_{50} values of unit density particles for the various impactor stages.

Clearly the size range covered by each stage increases with larger sizes.

3.2 Experimental Method

A single deposition experiment consisted of a two minute sample drawn through the blank line followed by a two minute sample through the model and ended with another two minute sample through the blank line. These times where measured on a stop watch and the three way valve was manually controlled to direct the flow. The ELPI saved data every second during the experiment. Each two minute time interval was further divided with a 40 s period at the beginning of the interval and a five second period at the end of each interval both being discarded to eliminate effects from settling of the instrument and errors in valve switching synchronization. This left a 75 s period of data which was actually used in each two minute interval. This

was sufficient to allow averaging of many breathing cycles yet short enough to allow many measurements to be taken. The ELPI provided an average concentration or count rate for size ranges corresponding to each stage of the impactor for each time interval. Nasal deposition for each impactor stage size range was calculated as the difference between the average number seen through the blank line at that stage and the average number seen through the model at that stage divided by the average number through the blank line at that stage.

This kind of relative measure should cancel a number of effects that would otherwise have caused errors in an absolute measure. The losses in the sampling line and the model line (which were of the same length) should be equal and are cancelled in the relative measure. Losses in the charger of the ELPI are calibrated into the reading of the machine but are also common to both paths. Because these charger losses can be very significant for larger particles the relative method of measurement is an advantage since it is less dependant on the accuracy of the correction within the ELPI. The type of measurement stored by the ELPI, counts or concentration, also did not matter when taking this kind of relative measure.

This method of measurement assumes that the concentration of aerosol in the chamber is constant with time. Strictly speaking this is not truly required since, by sampling before and after taking aerosol through the model, we can get accurate results even when the aerosol concentration is changing linearly in time. Between experiments and especially after having opened the chamber to change models sufficient time would be allowed for the concentration, as observed via the sample line, to return to a steady state. Generally, breathing patterns were ordered in an ascending or descending order of average flow rate in order to reduce the time needed to reach a steady state after switching breathing patterns.

There were a number of important findings contributing to this setup that I will mention in hopes they will be useful to others.

- High concentrations of the aerosol could be used as a marker under bright light to visualize the flow into or out of the model.

- The use of a mixing fan (computer case fan) was very important to ensure an

even aerosol concentration in the chamber to prevent position dependence of the model or sampling line.

- The nebulizer was positioned immediately adjacent to the chamber since losses of larger particles through a neutralizer and primary mixing chamber were too large to allow sufficient particles for filtration measurement.

- The nebulizer was operated at a very low pressure such that the jets would appear to start to spit in order to produce a very wide range of particle sizes. This also reduced the concentration of aerosol in the chamber so that the ELPI could be operated in its most sensitive range and several experiments could be performed between cleanings.

- The one way valve which samples only the inhale portion of the breathing cycle from the chamber avoids a large number of problems with supplying a meaningful sample to the ELPI. This is especially important with the small tidal volumes used for infants.

- Placing a rotameter or other flow measuring device in the path of the makeup air to ensure that it remains well matched to the ELPI flow is useful.

- The diameter of the sampling line should be carefully considered so that it provides an unbiased sample. It is possible in this case that 15 mm ID sampling line was too small since the data at the largest ELPI stage proved to be unreliable.

- Rigid piping is to be preferred to tubing in the common path to the ELPI since repositioning the tubing can change the losses of the system during a measurement.

- The in-house breathing machine has no pressure transducer or other feedback so operates based on displaced volume only. Since the air in the chamber of the breathing machine must be at higher than room pressure to force air out through the connected piping and apparatus and must be at lower than room

41

pressure to draw it back in, a compression or evacuation is required with every movement of the breathing machine. This compression or evacuation means that the volume displacement rate of the piston does not directly reflect the volume flow rate of the air at the point of interest. This problem is less severe if the piston is operated with the cylinder at minimum volume and more severe if the piston is operated at full volume since the percent volume change (relative to the tidal volume) needed to develop the required pressure is smaller in the former case and larger in the latter.

- Washing of the models to perform assays was complicated by the small and complex internal geometry. It was difficult to develop confidence that the inner surface could be well washed with a reasonable amount of solvent. Assays were not used for the measurement of deposition.

- It did prove feasible to mix vitamin E with sunflower oil in known ratios to produce a mixture which could be both nebulized and quantified using high pressure liquid chromography.

Five repeats of each measurement were made. Attempts were made to change conditions which should not affect the measurement such as the position of the model and sampling line, the order of breathing patterns used and time since last ELPI cleaning during these repeats. The average standard deviation for the repeats was 0.00749 or 0.749% indicating that the results were very repeatable.

3.3 Breathing Patterns

A full sinusoidal breathing pattern was produced by the breathing machine but a one way valve redirected the exhale flow to the room so that the model and sampling line only experienced inhalation flow. This prevented a large number of sampling problems including:

- Lack of aerosol sampling due to the dead space exceeding tidal volume.

42

- Problems with dead space mismatch between the model path and the sampling path. If these volumes are mismatched, and both inhale and exhale flows are used, actual sampled volumes will differ between the model path and the aerosol path. If these volumes are mismatched, and only the inhale flow is used, the mismatch will only create a sampling difference at the beginning of the measurement.

- If there is different filtration for different parts of the breathing flow only the first portion of the flow will be sampled by the ELPI if both the inhale and exhale flows are used. The filtration of the first part of the inhale curve may be different than the average filtration over the whole curve.

Overall deposition was low for the size of particles used. Breathing patterns were used that had larger than rest flow rates in order to get meaningful deposition measurements.

Nominal parameters for the breathing patterns used are given in Table 3.2. Actual patterns were captured, using the serial interface of the flow meter, for each experiment and used for calculation of average flow rate. An example of such a set of waveforms is shown in Figure 3.3. Clearly there is a small change in flow due to the added resistance of the model. The difference in sampled volume this causes was corrected for when the deposition was calculated.

Vt (cm^3)	bpm	$\bar{Q}$ (cm^3/s)
60.9	45	91.3
113.8	30	113.8
107.3	45	161.0
87.9	57	167.1
186.2	30	186.2

Table 3.2: Typical Breathing Patterns (Inhalation Only) Vt: tidal volume, bpm: breaths per minute, $\bar{Q}$: average flow rate during inhalation $\bar{Q} = 2 * Vt * bpm * 1min/60s$

Average weight for the infants in this study ranged from 6 kg to 11 kg as estimated from standard growth charts based on age and gender [13]. Resting tidal
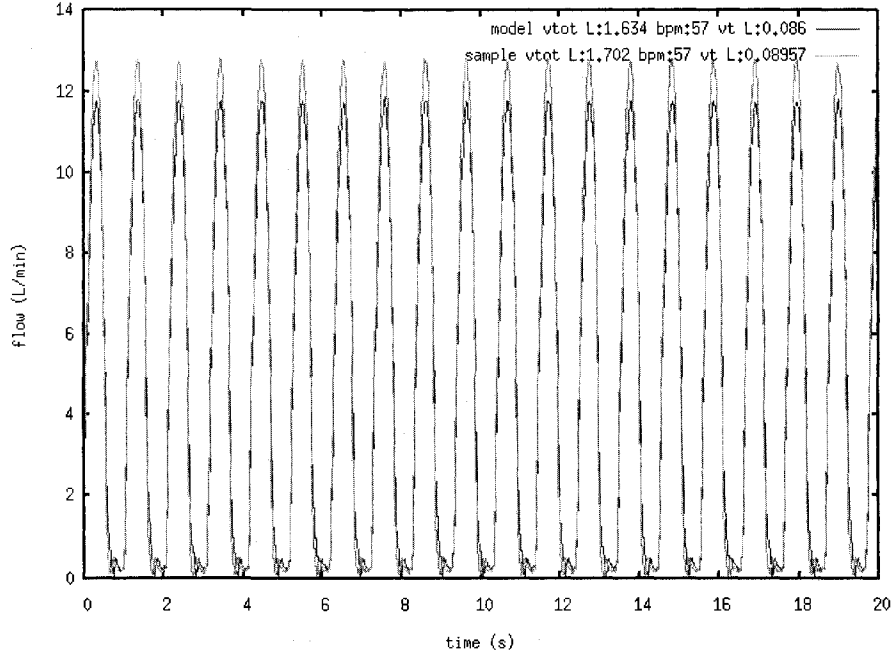
Figure 3.3: Captured Breathing Waveforms

volume ranges from 5 mL/kg to 8 mL/kg with age for this group[7]. This gives a resting tidal volume range of 30 mL to 88 mL for the present subjects. Resting breathing rate ranges from 44 bpm to 34 bpm with age from 2 months to 18 months [10]. Rosenthal[39] examined 23 children aged 8-10.5 yrs and found an increase in breathing rate of 97% from that at rest versus maximum exercise for boys in this age group, while girls increased breathing rate on average by 79%. In the same study, tidal volume was found to increase 185% for boys and 135% for girls under maximum exercise. The largest tidal volume used in the breathing patterns for the present study was a 112% increase from resting volume while the highest breathing rate used was a 26% increase from resting range. Extrapolating from Rosenthal[39] the breathing patterns used in the present study should be considered to represent states of moderate activity. As mentioned these higher breathing rates were necessary to generate meaningful deposition for the particle sizes used.

3.4 Calculating Deposition

The data for each experimental run consisted of an ELPI file with six minutes worth of samples at one second intervals, a portion of the volumetric flow pattern through the sample line recorded at 20 ms intervals, a portion of the volumetric flow pattern through the model recorded at 20 ms intervals (see Figure 3.3) and some notes on the conditions under which the experiment had been performed (position of model, nominal breathing pattern, subject number, run number).

The data from each run was placed in its own directory and pre-processing was performed on these raw files using a set of scripts to convert them into a GNU Octave (www.octave.org) data format.

Particle size was taken from the calculated geometric centres of each stage provided by the ELPI software. The available stage centre aerodynamic diameters (μm) are shown in Table 3.3.

Stage	1	2	3	4	5	6
$d_{ae}\mu$m	0.041	0.072	0.123	0.230	0.331	0.506
Stage	7	8	9	10	11	12
$d_{ae}\mu$m	0.795	1.282	2.033	3.212	5.330	8.407

Table 3.3: Geometric aerodynamic centres for each impactor stage.

The top stage and stages below 0.7 μm in aerodynamic diameter were discarded in all cases. For a single experiment any stage which had recorded zero counts was discarded since the use of that stage could lead to an under-estimation of particle deposition.

The average flow rates through the model and sample lines were calculated based on the flow through the breathing machine captured using a mass flow meter.

Each experiment consisted of two minutes of data from the sample line, two minutes through the model and a final two minutes through the sample line. The ELPI data for each impactor stage was split into time intervals corresponding to these portions of the experiment. The first 40 s and last 5 s of each time interval were discarded to allow for error in the synchronization of the three way valve and

45

to allow the ELPI to reach a steady state. The measured concentration from the two sampling intervals on either side of the model period were combined and averaged over time. The concentration as measured through the model was also averaged over time.

Figure 3.4 shows the division of the concentration data from a single impactor stage into sections representing the measurement through the model and through the sampling line.
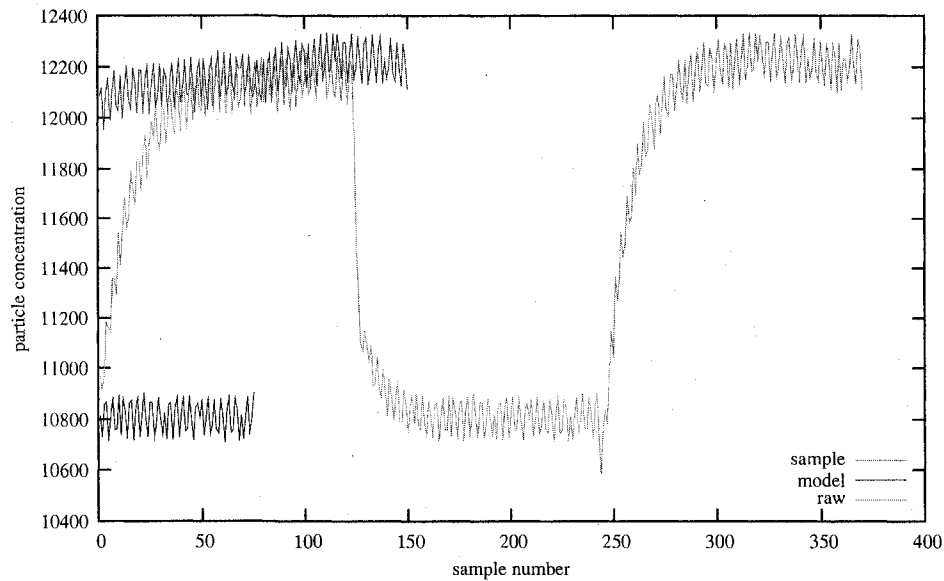
Figure 3.4: Splitting of concentration data.

The concentrations through the sample line and the model were corrected for any difference in average flow rate through the model and sample line.

Deposition fraction was calculated for each experiment and impactor stage as:

$$\eta = \frac{[sample] - [model]}{[sample]}$$

The repeats of each experiment where then averaged so that 275 data points were produced corresponding to 5 flow rates x 5 particle sizes x 11 subjects. The 5 particle sizes were identical for all flow rates and subjects while the flow rates were the

actual averages over the repeats and were different for each subject due to differences in nasal resistance.

3.5 Setup Validation

A few tests were performed to validate the experimental setup:

- No deposition was measured when the model was absent from the setup.

- Mixing was tested by positioning the sampling inlet at different places in the chamber and measuring the concentration. The model and sampling line were also often repositioned during repeats with no significant effect.

- The mass reported by the ELPI was compared with mass assay of the material on the collection plates for a set of sample runs at various concentrations and the same duration. This is not a valid absolute test since the losses in the charger are calibrated into the ELPI's measurement while that mass is strictly missing on the plates. Correction for losses by diffusion would also create some small differences but these would not likely be measurable by mass assay. This test did show that the relative measurement from one concentration to the next was consistent between the ELPI and the mass assay. It also showed that, for larger particles, the losses in the charger, as corrected by the ELPI, were significant with more than 90% of mass being lost in the charger.

- Some nasal deposition runs were performed with mono-disperse aerosol sized using the Aerosizer (TSI, Shoreview, MN) and these seemed to fall on the same curve as produced by the polydisperse source characterized by the ELPI. This is shown in Figure 3.5.

Calculations were also performed examining particle settling and sampling conditions for the sampling line. By comparing the settling velocity of the largest particles of interest to the residence time of the particles in the sampling system some estimate of the likely losses due to settling can be made. The terminal settling ve-
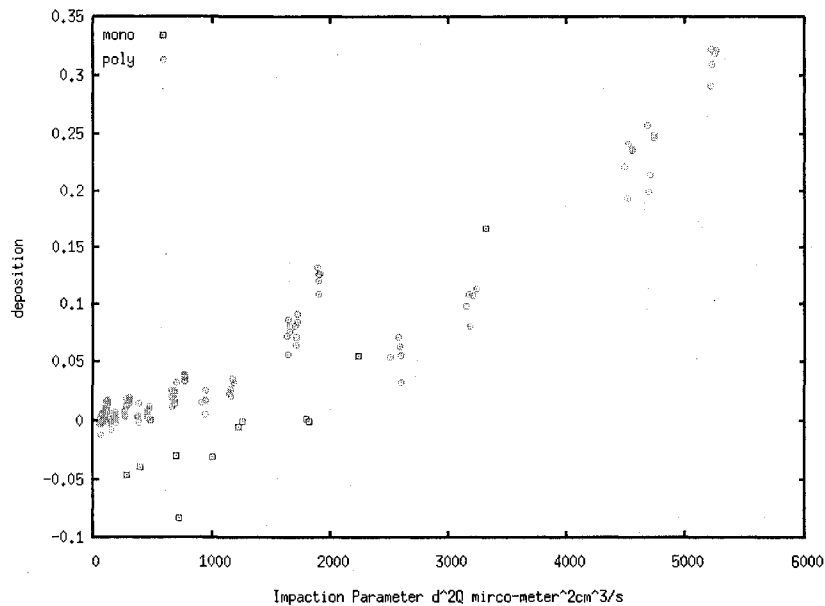
Figure 3.5: Monodisperse and polydisperse deposition for subject 2

locity can be found by equating the Stokes drag force to the weight of an aerosol particle. This gives the formula:

$$V_{settle} = \frac{\rho_{particle} g d^2}{18\mu}$$

By taking the largest particles of interest (6 μm with density 0.92 mg/ml) a settling velocity of 1.02e-3 m/s is obtained.

The residence time in the sampling system can be estimated as the volume of the sampling system divided by the average flow rate through the system. In the present case the sampling line had an inside diameter of 15 mm and was 0.4 m long. This gives a volume of 70.68 cm³. The lowest average inhale flow rate used in this study was 91.3 cm³/s. The average flow rate through the sampling system would be half of this or 45.6 cm³/s, since the inhale flow occupies half of the time cycle with no air flow during the other half cycle. This gives a residence time of 1.55 s. The distance a particle would fall in this time can then be estimated as 1.55 s*1.02e-3 m/s or 1.58 mm. This is much smaller than the tube diameter so it is safe to say that the losses in the sample line due to settling were small. In addition

48

the losses in the two matched lines should be equal so that losses due to settling in the sampling system should be taken into account through the differential method of estimating deposition.

Two conditions are suggested by Brockmann[31] when sampling from still air. One is that the particle Stokes number when sampling must be small so that all particle sizes can follow the stream pattern created by the sampling nozzle. The other is that the settling velocity must be small compared to the velocity in the sampling nozzle. This ensures that the sample will be largely independent of the orientation of the nozzle (with respect to gravity). The following criteria are suggested by Brockmann:

$$\frac{V_{settle}}{U_{nozzle}} < 0.04$$
$$Stk < 0.016$$

Since both the Stokes number and the settling velocity are proportional to d^2 these conditions are hardest to satisfy for the largest particle sizes. The Stokes condition will be hardest to satisfy at the largest flow rates while the settling velocity condition will be hardest to satisfy at the lowest average flow rates. The lowest average inhale flow rate used was 91.3 cm^3/s which corresponds to an average sampling rate of 45.6 cm^3/s. The highest average inhale rate was 186.2 cm^3/s. By dividing the flow rate by the nozzle area we can compute the nozzle velocity. The sampling line cross-section is 1.77 cm^2. The lowest nozzle velocity is then 25.8 cm/s or 0.258 m/s. Using the settling velocity computed earlier of 0.00102 m/s we find a ratio of $\frac{V_{settle}}{U_{nozzle}}$ =4e-3 which is less than 4e-2.

The Stokes number for the largest particle is computed using:

$$Stk = \frac{U_{nozzle}\rho_{particle}d^2}{18\mu D}$$

If we want to look at the worst case Stokes number we should consider the maximum instantaneous velocity. The peak flow rate for the flow pattern resulting in an average inhale flow rate of 186.2 cm^3/s is approximately 290 cm^3/s. This gives a peak nozzle velocity of 1.65 m/s. The Stokes number using this velocity, a particle size of 6 μm and density 0.92 g/ml is 0.01 satisfying the Stokes condition.

3.6 Pressure Drop Measurements

Pressure drop measurements were performed under steady flow conditions for all models. Differential pressure between the room and outlet of the model was measured (HHP-103, Omega, Stamford, CT) while the flow rate was measured using a mass flow meter (4143 series, TSI, Shoreview, MN). These flow rates were taken to cover the range of average flow rates used in the deposition experiments.

The measurements of pressure drop also give additional information about the Reynolds dependence. The non-dimensionalized pressure drop is plotted against Reynolds number for each model in Figure 3.6. The pressure drop is non-dimensionalized to give the main flow kinetic energy that is imparted by the pressure difference. This quantity is also closely related to the Darcy-Weisbach friction factor. This shows that the amount of drag in the model is changing with Reynolds number in a non-linear fashion. This indicates that the flow pattern is likely changing with Reynolds number in the flow range used for these experiments. The length scale used to non-dimensionalize pressure and to define Reynolds number is airway volume divided by airway surface and is discussed in the next chapter.

This style of plot is sometimes called a Moody diagram and can be used to compute the drag co-efficient for standard geometries. In the Moody diagram for a pipe the non-dimensionalized pressure drop will be nearly constant at high Reynolds numbers indicating that the flow is fully turbulent. The the location of the transition region and the drag at high Reynolds number depend on the roughness of the pipe surface. A Moody diagram for work with pipes of various roughness is shown in Figure 3.7 courtesy of the Glasgow College of Nautical Studies [37].

The Moody diagram has also been used to characterize the steady and unsteady flows in the central airways by Isabeya and Chang[19].

3.7 Raw Data

The raw data generated by the deposition experiments were deposition, average flow rate, particle size triplets. This raw data (averaged over repeats) is shown in
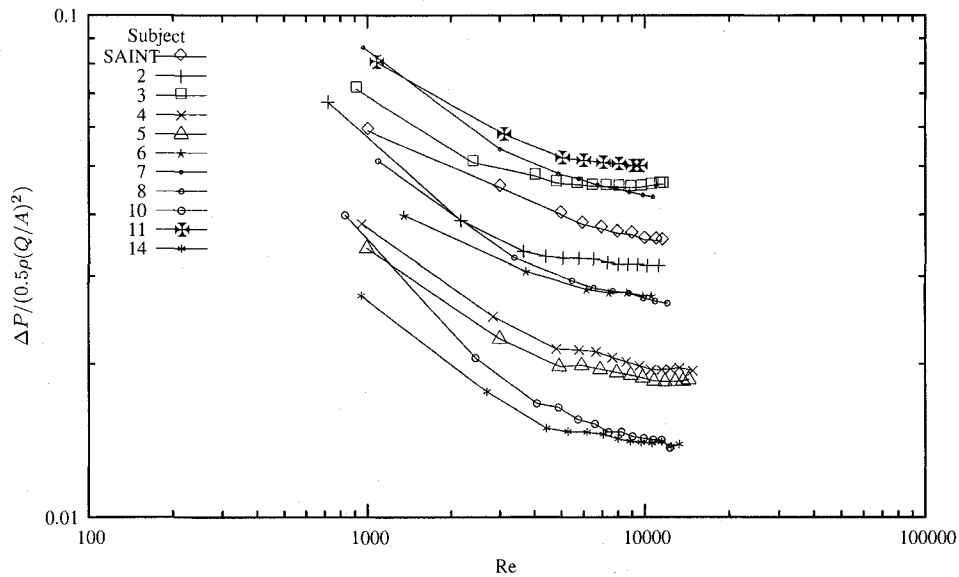
Figure 3.6: Pressure drop vs. Reynolds number

in Figures 3.8 and 3.9 and is tabulated in Appendix A. These two figures can be considered two-dimensional views of what is a three-dimensional data set ie. the x,z and y,z views of an x,y,z data set. No distinction is made in these figures between the data from different subjects.

Figure 3.8 shows aerosol deposition versus average flow rate of each of five breathing patterns. Each point on the figure is assigned a symbol based on the particle size used to generate that data point. From this figure it is clear that the deposition has a strong particle size dependence with the larger particle sizes showing higher deposition. It is also clear that there is a great deal of inter-subject variability based on the broad spreading of the points of the same symbol at each flow rate. The overall deposition is seen to increase from left to right with flow rate.

Figure 3.9 shows aerosol deposition versus particle size with different average flow rates appearing as different symbols. The average flow rates of 161.0 cm^3/s and 167.1 cm^3/s have very similar deposition even though the tidal volumes and breathing rates used to generate them were quite different. The strong dependence

51

of deposition on particle size is again apparent from left to right in this figure. While there is a tendency for the larger flow rates to have higher deposition this trend is somewhat obscured by the inter-subject variability.

It should also be mentioned that the data from the top stage of the ELPI was discarded. The data from the top stage appeared as significant outliers in the data set with lower than expected deposition and were believed to be incorrect. Whether this is due to the actual distribution of particle sizes within the large size range of this stage not being log normal or to some sampling problem is not known.

Deposition is shown versus impaction parameter in Figure 3.10. Here each subject has its own symbol. The inter-subject variability is quite evident but even the deposition for a single individual does not fall on a single curve.

Deposition versus impaction parameter for subject 5 is plotted separately in Figure 3.11 where the different flow rates are assigned different symbols. This clearly highlights the fact that a different deposition curve exists for the different average flow rates used. This suggests a dependence on flow rate beyond the Stokes number.

The steps taken to collapse the data shown in Figure 3.10 is the subject of the next chapter.
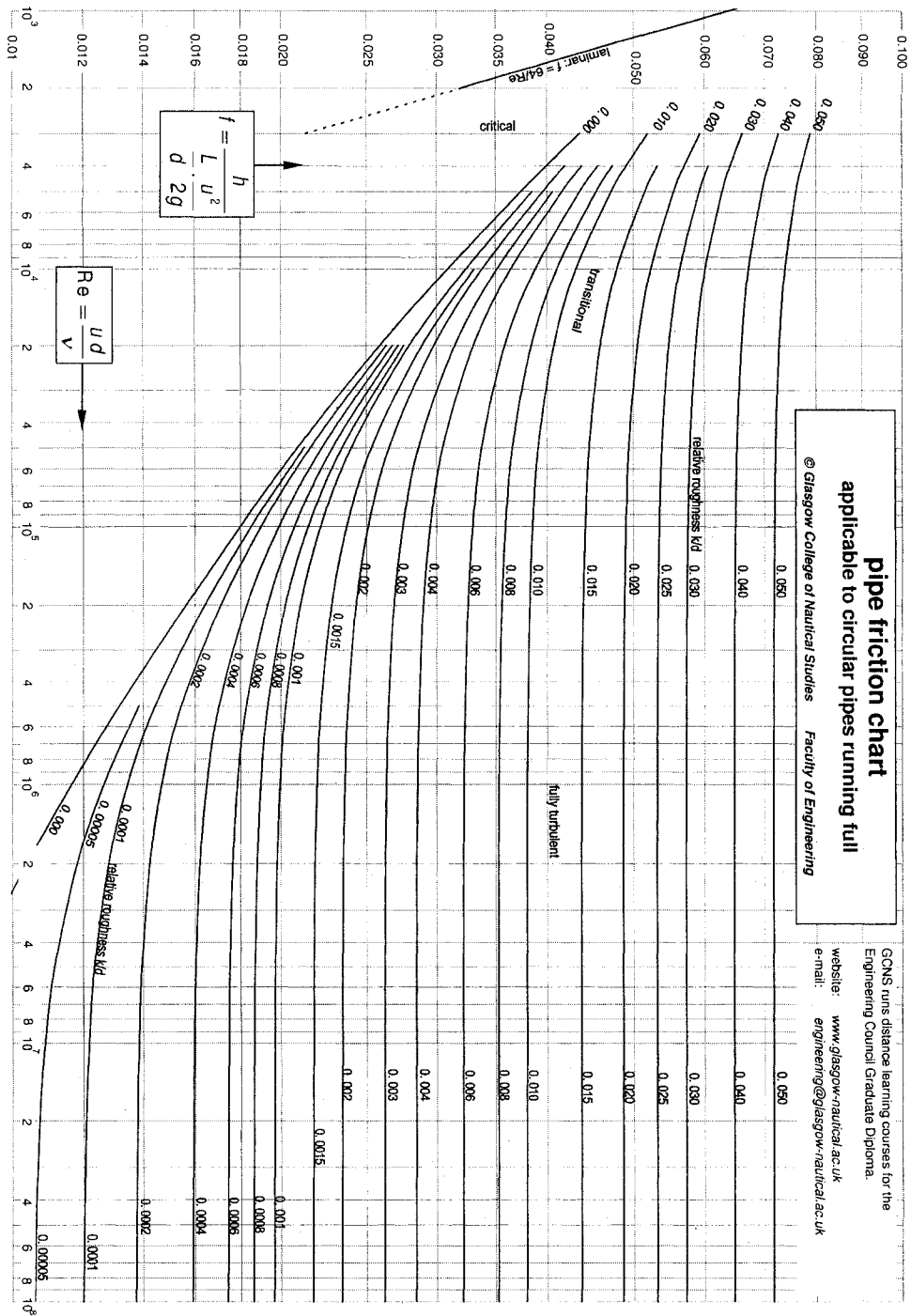
Figure 3.7: Moody Diagram courtesy Glasgow College of Nautical Studies[37]
(reprinted with permission)

53
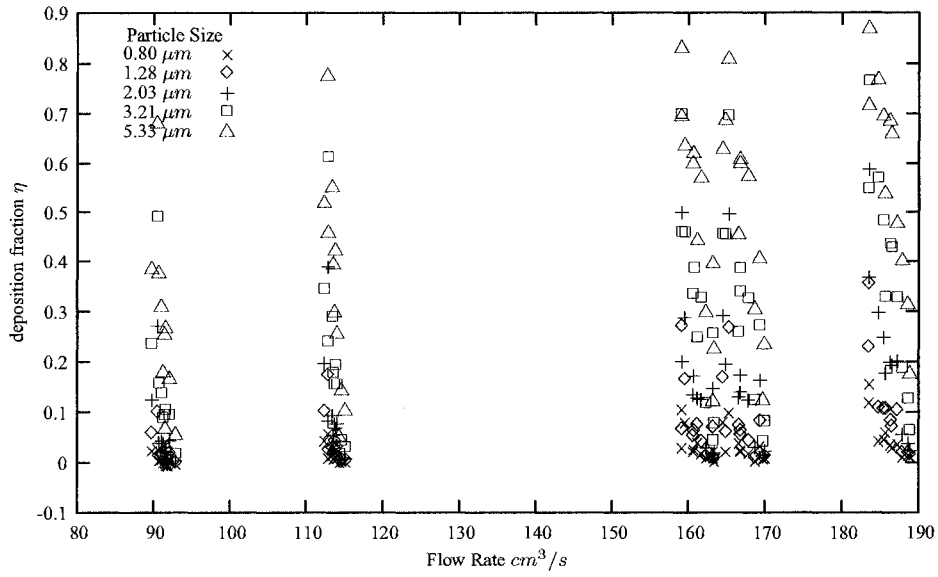
Figure 3.8: Deposition vs. Flow
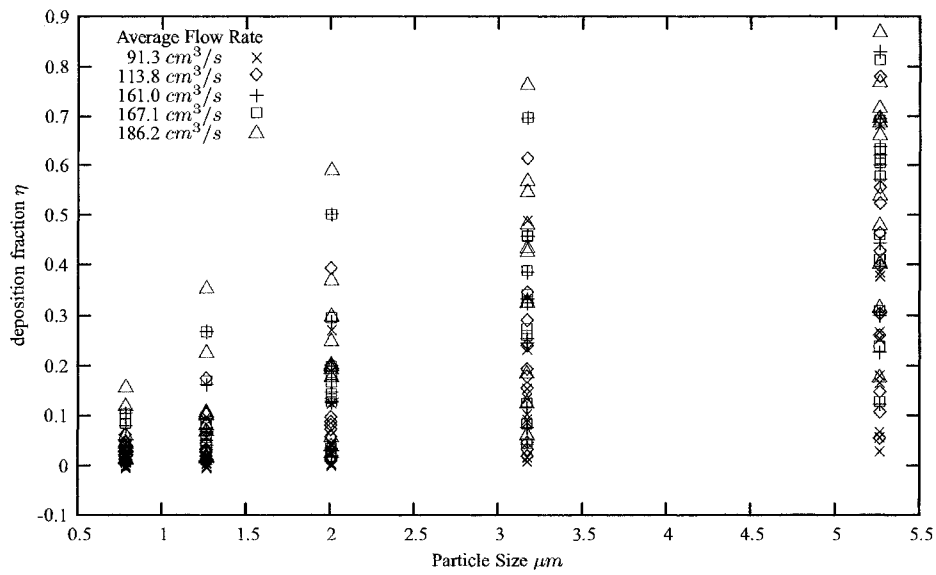
Figure 3.9: Deposition vs. Particle Size

54
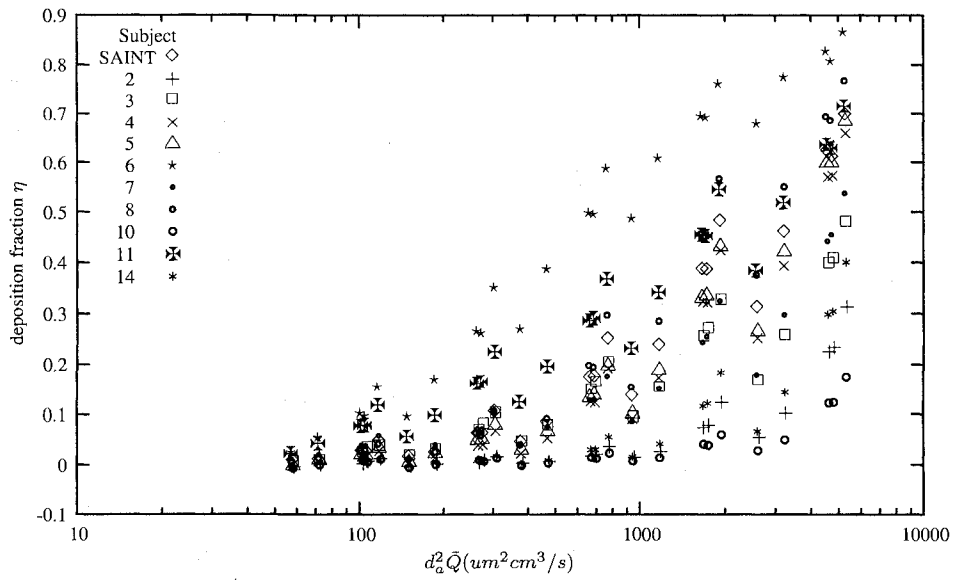
Figure 3.10: Deposition vs. Impaction Factor
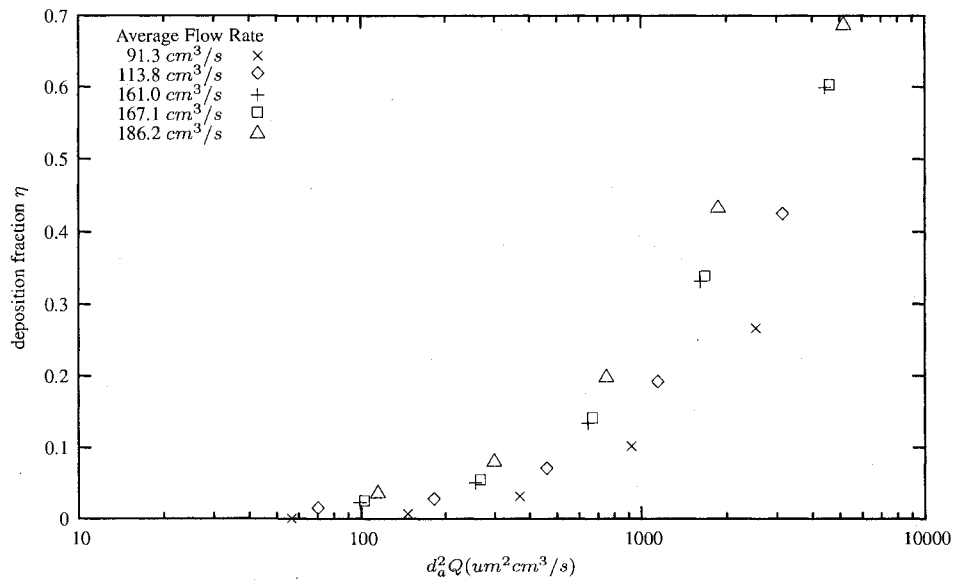
Figure 3.11: Deposition vs. Impaction Factor Subject 5

Chapter 4

Constructing Correlations

4.1 Data Analysis

The data for single individuals was plotted against impaction parameter $(d_{ae}^2 \bar{Q})$ which is proportional to Stokes number for any individual. The data did not form a single curve but formed several curves depending on flow rate as seen for subject 5 in Figure 3.11. This suggested an additional flow rate dependence beyond the impaction parameter or Stokes number.

It is likely that the air flow pattern in the model is changing with Reynolds number and this is causing a flow dependence beyond the flow dependence in the impaction parameter. This is consistent with the pressure drops observed in Figure 3.6 which are changing with Reynolds number over the flow rates studied. It was possible to collapse the data for each individual by plotting against a function that combined dependence on d_{ae} and $\bar{Q}$ in a more flexible way for each subject as shown in Figure 4.1. In order to capture the inter-subject variability and collapse the data onto a single curve the correct dimension or dimensions needed to be identified which could explain the coefficients used for each subject in Figure 4.1.

A number of different geometric factors where tried in order to account for the intersubject variability in deposition including airway length, average cross-sectional area, minimum cross-sectional area, pressure drop across the model and airway volume/airway surface area. Table 4.1 gives the r^2 values for fits using these parameters. Pressure drop and airway volume/airway surface area were combined
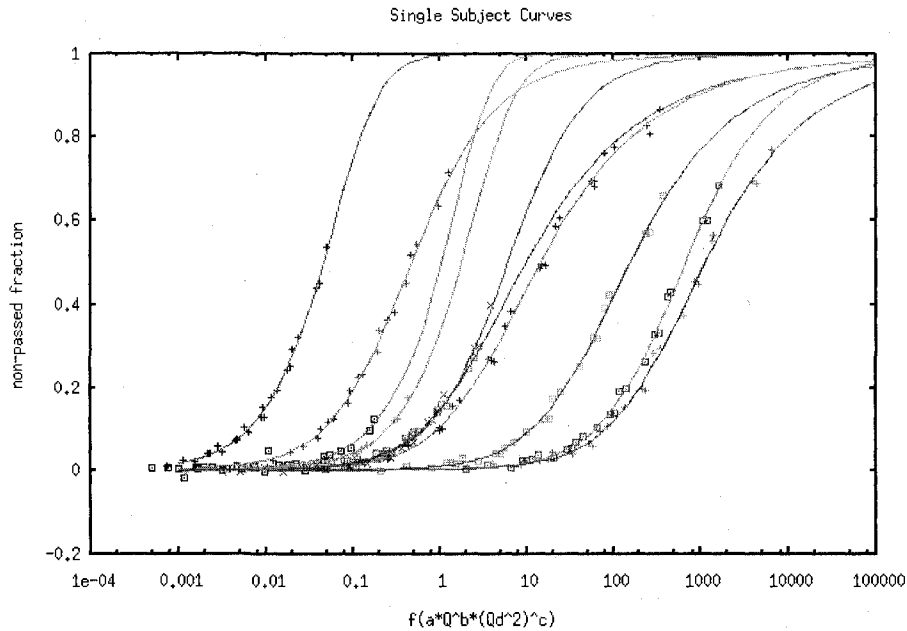
Figure 4.1: Fits for individuals with extra flow dependence.

to good effect as discussed below. An attempt was made to separate the models into anterior and posterior halves and fit the data using dimensions from each half separately with the idea that if the deposition was dominantly in the front of the nose the fits would be better if the dimensions from only this part of the nose were used. This actually produced a poorer fit than using dimensions from the entire replica.

In order to quantify the degree of collapse obtained with different dimensions a multi-parameter fit was used. Two parameters (a, b) gave the overall curve shape of the form $\eta = 1 - \left(\frac{a}{a+x}\right)^b$ where the x axis is determined by additional fit parameters and Stk; Re and Stk; or Re, Stk and D (a length scale), as part of a single fit. For example $\eta = 1 - \left(\frac{a}{a+Stk^c}\right)^b$ would be used as a fit function with the parameters a,b,c being determined for the entire data set at the same time.

All curve fitting was done using Levenberg-Marquardt nonlinear regression with a least squares objective function in the GNU Octave software package ver-

57

sion 2.1.72 (www.octave.org). Multiple starting points in the parameter space were used to ensure a reasonably global solution. Equal weighting was given to each data point during fitting.

Fit, D=	$\frac{V}{As}$	$\frac{V}{A_{min}}$	L	$\frac{As}{L}$	$\sqrt{\frac{V}{L}}$	$\sqrt{A_{min}}$	P	$\frac{1}{P}$
Stk, Re	0.887	0.745	0.545	0.606	0.792	0.495	0.351	0.753
Stk, Re, D	0.930	0.778	0.588	0.638	0.813	0.590	0.901	0.901

Table 4.1: r^2 values using various scale dimensions.

The length scale, D, which provides the best collapse of the measured data was found to be airway volume divided by airway surface area. This is apparent from an inspection of Table 4.1.

Table 4.1 gives the r^2 values of the best fits obtained using the dimension D as calculated using the formula in each column header. This value of D was used to calculate Re, Stk. The dimensionality of Re, Stk calculated using pressure or 1/pressure as a dimension is not strictly correct but can be considered to represent a physical dimension that scales with pressure drop. The first row of the table gives the best fits obtained using a formula of the form shown in Equation 4.1 while the second row gives the best fits obtained using a formula of the form shown in Equation 4.2.

Hydraulic diameter is often used as a scale dimension in non-circular geometries and is defined as:

$$D_h = \frac{4*area}{perimeter}$$

By comparison, D has some analogy to the hydraulic diameter for these geometries which vary in cross-section along their length since it is equivalent to:

$$D = \frac{average\ area}{average\ perimeter}$$

If deposition is plotted versus Stokes number as in Figure 4.2 the scatter is reduced compared to Figure 3.10 since there is some correction for the individual

58
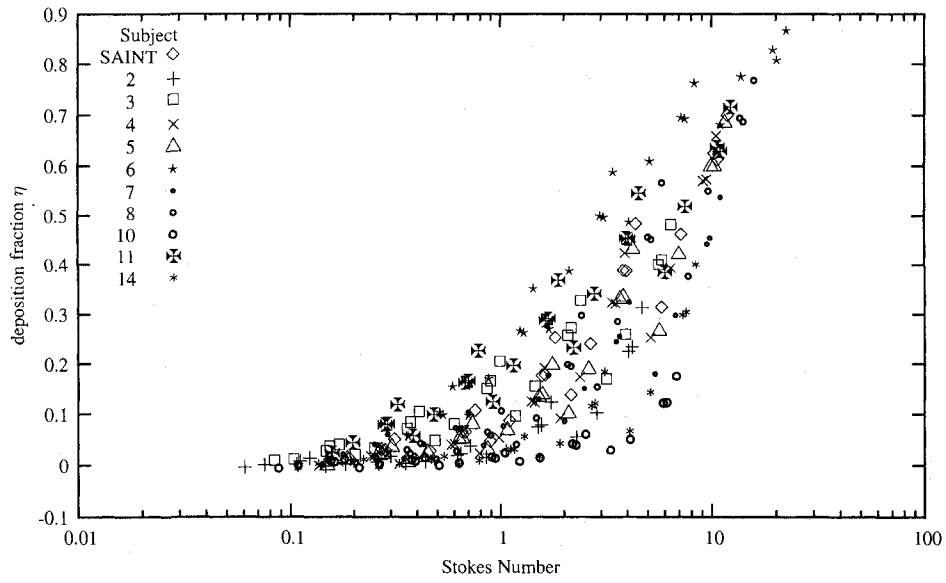
Figure 4.2: Deposition vs. Stk
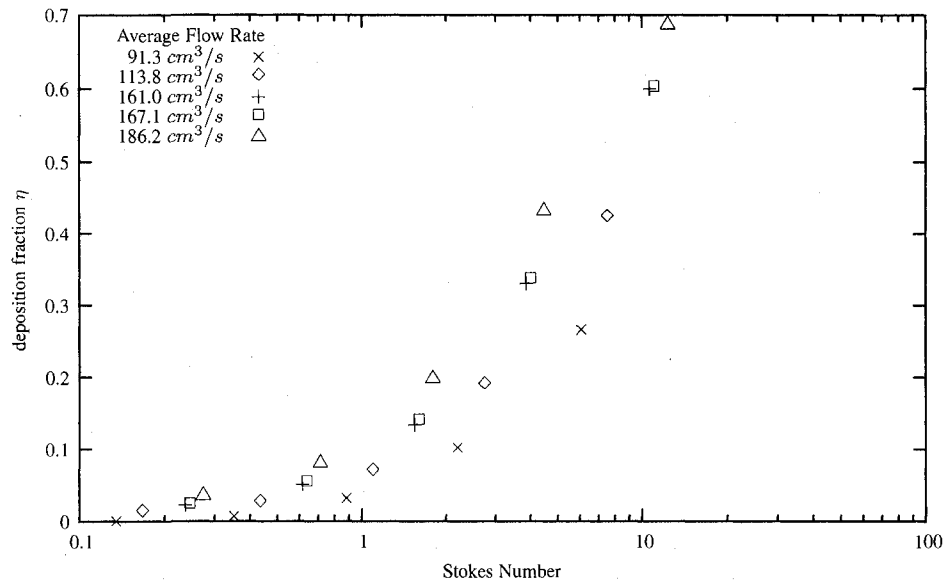
Figure 4.3: Deposition vs. Stk Subject 5

59

dimensions of different subjects, however deposition for single subjects still fall on different curves for different flow rates as seen in Figure 4.3 for subject 5.

If a single best fit is calculated for all deposition where the x-axis is a function of Re and Stk such that $x = Re^c Stk^d$ where c and d are fit parameters, single curves for each individual result and the scatter of the plot for all individuals is reduced further. This is shown in Figure 4.4. The individual model dimension D is included in both the Reynolds number Stokes number.
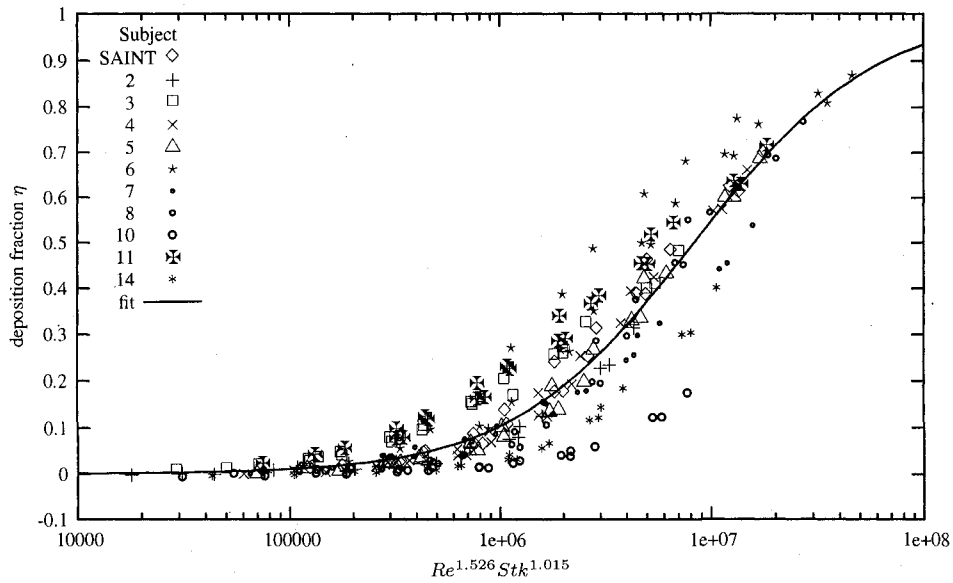
Figure 4.4: Deposition vs. f(Re,Stk)

The formula for the fit function shown in Figure 4.4 is:

$$\eta = 1 - \left(\frac{10072000}{10072000 + (Re^{1.526} Stk^{1.015})} \right)^{1.126} \tag{4.1}$$

Many non-dimensionalized numbers have the same meaning for different scales of the same geometry since the scale is explicitly included in the non-dimensionalized number. In the case of infant nasal airways the geometries are not scaled versions of each other but each one is unique with its own physical detail (see Figure 2.6).

The basic shape is the same but the finer features differ. In such a case the non-dimensionalized parameters can not be expected to fully capture the flow characteristics across geometries. For example the flow pattern at a given Reynolds number (which is based on a single nasal dimension) is not expected to be the same in two different nasal passages. While some collapse was obtained in Figure 4.4 using a function of Re and Stk we would not expect this to fully collapse the curve since these factors do not account for differences in the nasal geometries that are not captured by our scale factor D.

In order to better predict deposition an empirical fit was attempted which included Stokes number, Reynolds number and an additional dependence on the length scale D defined as airway volume/airway surface area. The best fit using these parameters is shown in Figure 4.5. Adding the additional dependence on length scale, D, generates a predictive curve that better matches the observed deposition. This additional dependence on D could be viewed as a correction to the D factor. The geometric factor which is best suited to defining Reynolds and Stokes may not be airway volume/airway surface but something related to this through a power. The additional dependence on D could be seen as the relationship between D and a better geometric factor. In addition, the best single geometric factor for Reynolds number and Stokes number is not necessarily the same so if you view the additional D dependence as a correction that correction may not be applied equally to Reynolds and Stokes.

The formula for the fit shown in Figure 4.5 is:

$$\eta = 1 - \left(\frac{216390}{216390 + (Re^{1.118} Stk^{1.057} (D/Davg)^{-2.840})} \right)^{0.8510} \tag{4.2}$$

where $D = \frac{V}{As}$, $Davg$=1.20mm.

Equation (4.2) allows quantitative prediction of nasal deposition in individual infant subjects. Comparing infant nasal deposition from equation (4.2) to that seen in adults [5] for subjects at rest we find less nasal deposition in infants. e.g. for d=2 μm, $\bar{Q}$=72 cm^3/s (4.3 L/min), D=$Davg$, $\rho_{particle}$=1000 kg/m^3 equation (4.2)
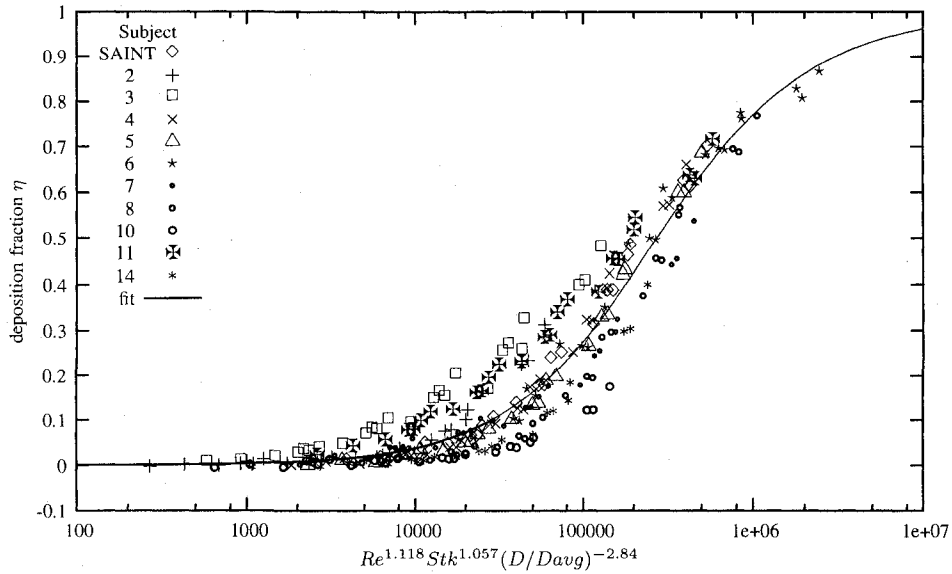
Figure 4.5: Deposition vs. Non-dimensionalized parameter

gives $\eta = 2.0\%$ for an infant, while the nasal deposition correlation of Cheng [5] gives $\eta = 18.2\%$ (assuming a resting adult flow rate of 15 L/min [39] and taking A_{min} of 2.08 cm^2 as given by Cheng). The difference in resting flow rate between infants and adults is, of course, a large factor here.

A slightly better fit (r^2=0.948) can be obtained if Reynolds number and Stokes number are defined using the dimension D as discussed previously and if the pressure drop across the models at 7 L/min is added to the fit as an empirical correction in place of an additional dependence on D. The resulting curve is shown in Figure 4.6. The pressure drop adds additional information to the fit and produces a tighter collapse but it also requires an additional measurement to be made in order to use the fit to predict deposition.

The equation for the fit shown in Figure 4.6 is:

$$\eta = 1 - \left(\frac{450150}{450150 + (Re^{1.255} Stk^{1.141} (P/Pavg)^{0.6483})} \right)^{0.6258} \tag{4.3}$$

where $Pavg$=151.78 Pa.
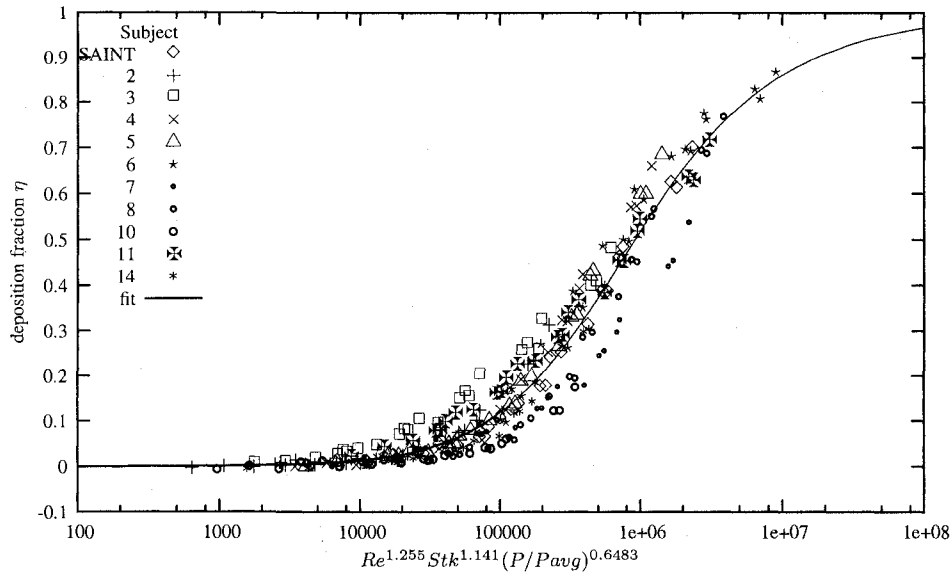
Figure 4.6: Deposition vs. Non-dimensionalized parameter (pressure)

Depending on the information available other modeling functions could be created to predict nasal deposition. In general more geometric information should allow a better prediction of deposition.

4.2 Model Sensitivity

Since Equation (4.2) represents a predictive model for nasal deposition we are interested to understand the sensitivity of the predictions to the supplied inputs. This model takes the Reynolds number, Stokes number and dimension D as inputs. Knowing the appropriate constants for fluid viscosity, fluid density and particle density, Reynolds number and Stokes number can be calculated if average flow rate ($\bar{Q}$), particle diameter and dimension D are known. Though it is not obvious in Figure 4.5, due to the log scaling of the x-axis, the slope of the deposition curve is greatest at small values of x. This is more obvious in a plot with a linear x-axis such as Figure 4.7. Selecting a point near a deposition fraction of 10% as a point that would have high sensitivity but high enough deposition to be of interest gives

a target x value about which to look at sensitivity.
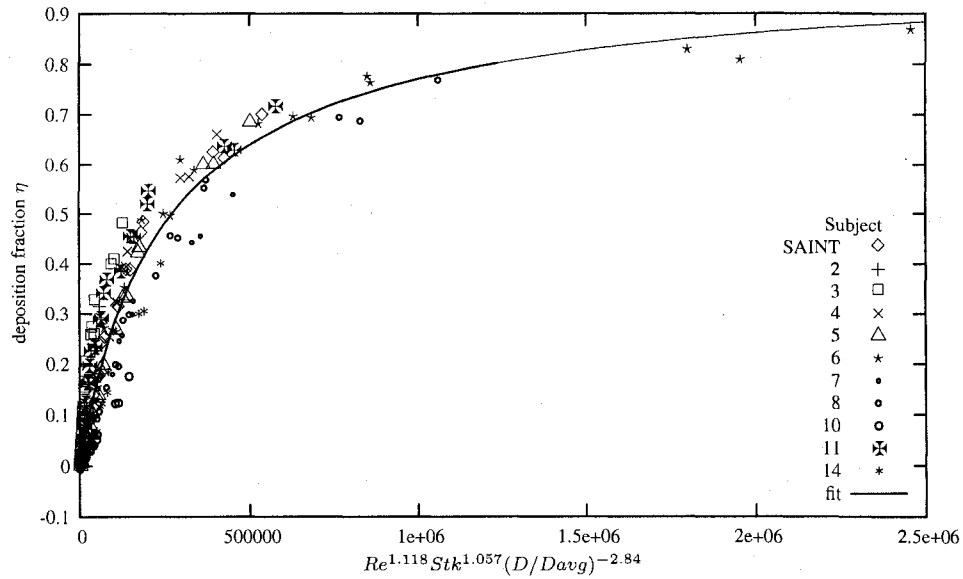
Figure 4.7: Deposition vs. Non-dimensionalized parameter (linear)

An infinite combination of $\bar{Q}$, particle diameters and length scales can be chosen which will provide the desired x value. To take a realistic case a 2 μm diameter particle and characteristic dimension of 1.2 mm are chosen. This requires a flow rate of 149 cm³/s to reach the desired 10% deposition. The three inputs were independently modified ±5% about this point and the predicted deposition calculated. These predicted depositions were plotted against the varying parameter in Figures 4.8, 4.9 and 4.10.

The sensitivity to the length scale D is the greatest while the sensitivity to the flow rate and particle dimensions is similar and smaller.
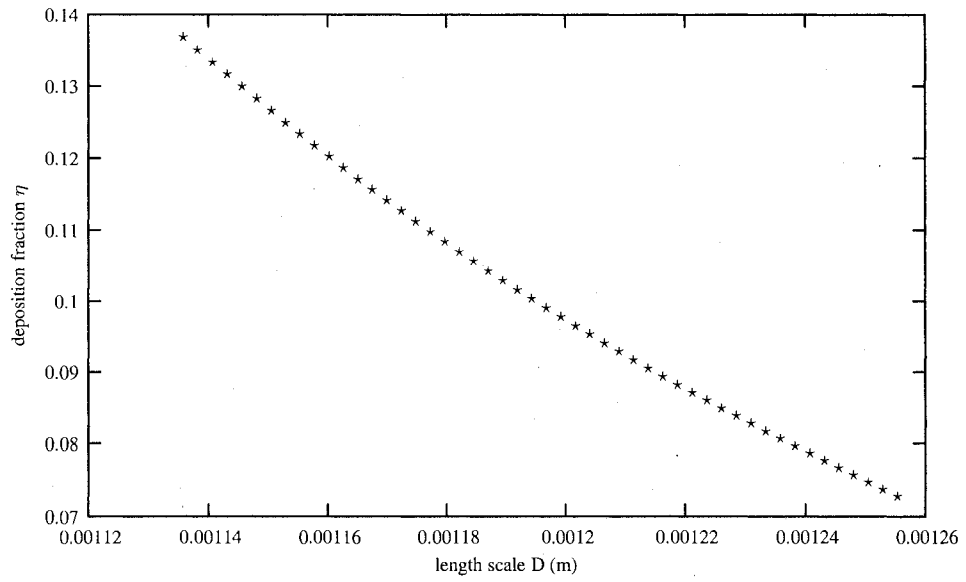
Figure 4.8: Predicted Deposition vs. Length Scale
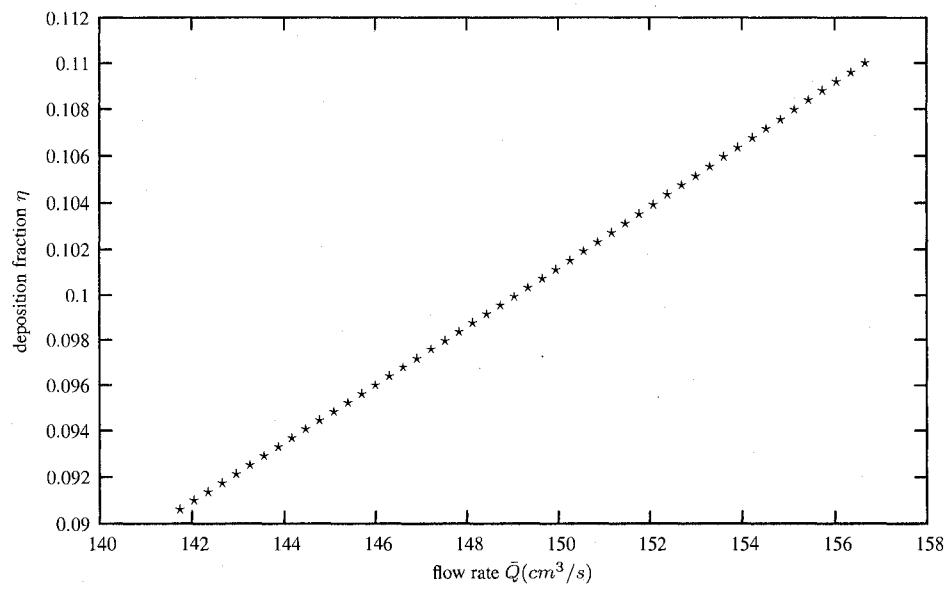
Figure 4.9: Predicted Deposition vs. Flow Rate

65
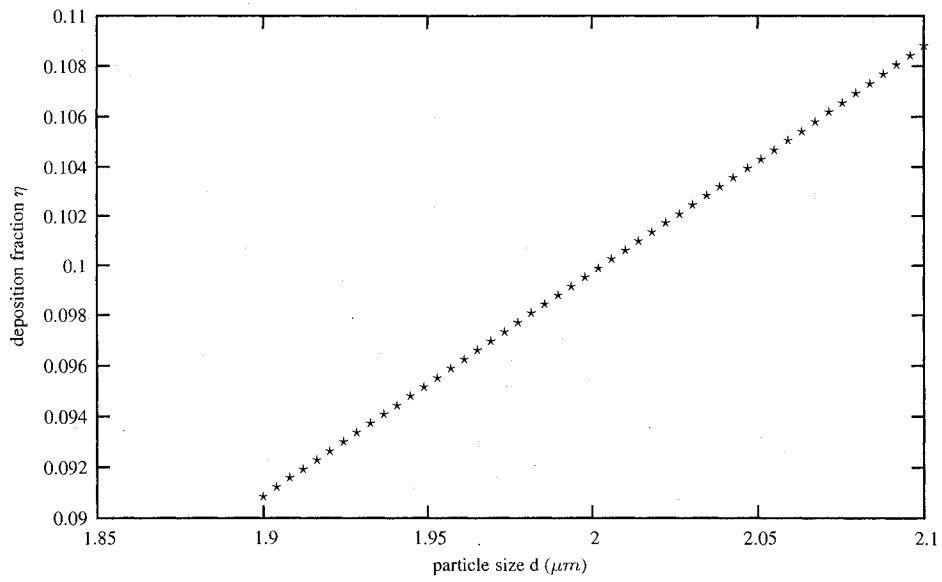
Figure 4.10: Predicted Deposition vs. Particle Diameter

Chapter 5

Conclusions

5.1 Scope

Aerosol therapy can be very effective at targeting various lung diseases that affect infants and children including asthma and cystic fibrosis. For very young children the nasal airway is an important route for aerosol delivery. This project aims at better understanding the filtration function of the infant nose and the parameters upon which it depends.

5.2 Findings

Models built from CT source data using rapid proto-typing technology can effectively capture the nasal geometry of infants. In the current case grey-scale thresholding, normalized smoothing and a build system using a wax support were employed. Some differences exist between the in vivo airway and the model but these differences are believed to be small when compared to inter-subject differences. These models can be used to perform in vitro experiments that would be difficult and expensive to perform in vivo.

Nasal deposition in infants generated using a periodic breathing pattern seems to be well described by the average flow-rate of that pattern. This is seen in very similar deposition for different combinations of tidal volume and breathing rate which give similar average flow rate.

Our measurements of nasal deposition in replicas of infants indicate that there is

a great deal of variability in nasal aerosol deposition between individual infants. See Figures 3.8, 3.9 and 3.10. Deposition within a single subject depends not only on Stokes number but also on Reynolds number. This is apparent from our deposition data (Figures 3.11 and 4.3) and consistent with our static pressure drop measurements (Figure 3.6) which appears to indicate changes in the air flow pattern with Reynolds number.

A reasonable predictive equation for deposition in all eleven subjects was obtained by including both Stokes and Reynolds numbers scaled using total nasal air volume divided by surface area. An even tighter fit was obtained by including an additional direct dependence on volume over surface area. The resulting equation,

$$\eta = 1 - \left(\frac{216390}{216390 + (Re^{1.118} Stk^{1.057} (D/Davg)^{-2.840})} \right)^{0.8510} \tag{5.1}$$

where $D = \frac{V}{As}$, $Davg$=1.20mm, allows estimation of nasal deposition in individual infants and is expected to be useful for those wanting to estimate the fraction of aerosol reaching infant lungs during nasal or mixed nasal/oral breathing. Hopefully this relationship can also provide useful guidance to those developing aerosol delivery devices and aerosol preparations for infants.

Characterization of the sensitivity of this equation to its inputs has been performed and is given in Figures 4.8, 4.9 and 4.10.

Other predictive functions can be generated depending on the available airway dimensional information.

5.3   Summary of Contributions

- Ten new infant nasal replicas have been constructed which are available for future studies.

- An experimental method was developed to rapidly measure deposition using the electronic low pressure impactor while employing small tidal volumes and realistic breathing patterns.

- A Reynolds number dependence on nasal deposition in infants was found.

- The single geometric parameter which best captures inter-subject variability was found to be nasal volume/nasal surface area which has some similarity to hydraulic diameter.

- A predictive correlation (equation 5.1) based on nasal volume/nasal surface area was found which can be used to predict aerosol deposition in infant airways.

5.4   Future Research

The data collected in the current study focussed on deposition by inertial impaction. Studies with particles of smaller size could be performed to confirm work done on diffusional deposition [6]. Based on a cursory examination of the data from all ELPI channels, particles of less than 40 nm in aerodynamic diameter should be targeted when looking at diffusional deposition in infant nasal airways.

The data we produced seemed to be well captured using the average flow rate for our breathing patterns. Further work could be done to determine if cyclical breathing adds value to in vitro nasal deposition studies [40].

Further age based studies are planned to see what parameters are necessary to explain nasal deposition in older children through to adults. It is hoped that a single correlation can be developed to predict nasal deposition for all ages.

Studies could be performed which would measure regional deposition in the infant nasal airway replicas. Some methods were considered to visualize regional deposition. Direct MRI of the oil droplets is likely not possible due to the small volumes of oil involved. The addition of MRI contrast agents to the the aerosol droplets has been discussed as a possible method of producing an image of regional deposition. A concern in using this method is the removal of the contrast agent from the convoluted airways after imaging has been completed. The construction of transparent models and the use of fluorescent dyes might be a feasible approach.

Transparent models would also allow flow visualization as was done by Hopkins et al[16]. This could be done as either a qualitative study or as a more quantitative

project looking at differences and trends among the geometries we have captured.

Computational fluid dynamics modeling could be performed on the captured geometries to try to replicate total deposition and gain insight into the air flow patterns and regional deposition within the nasal airways.

Experiments could be performed on scaled models to confirm the expected dimensional dependence and further investigate the effects of surface roughness by reducing the roughness relative to the airway dimension. In addition, the carrier gas density and viscosity could be changed to try to confirm the observed Reynolds number dependence.

Deposition measurements on models which had been highly smoothed in CAD could be performed to understand the effect of loss of fine detail in nasal modeling.

Bibliography

[1] MH Becquemin, DL Swift, A Bouchikhi, M Roy, and A Teillac. Particle deposition and resistance in the noses of adults and children. *Eur Respir J*, 4:694–702, June 1991.

[2] William D. Bennett, Kirby L. Zeman, and Annie M. Jarabek. Nasal contribution to breathing and fine particle deposition in children versus adults. *Journal of Toxicology and Environmental Health*, 71:227–237, 2008.

[3] Hans Bisgaard, Chris O'Callaghan, and Gerald C. Smaldone. *Drug Delivery to the Lung*. Informa Healthcare, 1 edition, October 2001.

[4] Y S Cheng, T D Holmes, J Gao, R A Guilmette, S Li, Y Surakitbanharn, and C Rowlings. Characterization of nasal spray pumps and deposition pattern in a replica of the human nasal airway. *Journal of aerosol medicine*, 14:267–80, 2001. PMID: 11681658.

[5] Yung Sung Cheng. Aerosol deposition in the extrathoracic region. *Aerosol Science and Technology*, 37:659–671, 2003.

[6] Yung-Sung Cheng, Shawna M. Smith, Hsu-Chi Yeh, Dai-Byung Kim, Kuo-Hsi Cheng, and David L. Swift. Deposition of ultrafine aerosols and thoron progeny in replicas of nasal airways of young children. *Aerosol Science and Technology*, 3:541–552, 1995.

[7] Victor Chernick, Thomas F. Boat, Robert W. Wilmott, and Andrew Bush. *Kendig's Disorders of the Respiratory Tract in Children (Disorders of the Respiratory Tract in Children*. Saunders, 7 edition, March 2006.

[8] Mathieu Desbrun, Mark Meyer, Peter Schroder, and Alan H. Barr. *Implicit fairing of irregular meshes using diffusion and curvature flow*. ACM Press/Addison-Wesley Publishing Co., 1999.

[9] P G Djupesland and B Lyholm. Changes in nasal airway dimensions in infancy. *Acta oto-laryngologica*, 118:852–8, November 1998. PMID: 9870633.

[10] Allen J. Dozor and Nikhil Amin. *Primary Pediatric Pulmonology*. Blackwell Publishing, 2002.

[11] J E Esposito-Festen, B Ates, F J M van Vliet, A F M Verbraak, J C de Jongste, and H A W M Tiddens. Effect of a facemask leak on aerosol delivery from a pmdi-spacer system. *Journal of aerosol medicine : the official journal of the International Society for Aerosols in Medicine*, 17:1–6, 2004. PMID: 15120007.

[12] Warren H. Finlay. *The Mechanics of Inhaled Pharmaceutical Aerosols: An Introduction.* Academic Press, 2001.

[13] Centers for Disease Control and Prevention. Growth charts weight-for-age percentiles. *www.cdc.gov/growthcharts*, September 2000.

[14] B. Grgic, W. H. Finlay, P. K. P. Burnell, and A. F. Heenan. In vitro intersubject and intrasubject deposition measurements in realistic mouth-throat geometries. *Journal of Aerosol Science*, 35:1025–1040, 2004.

[15] J. Heyder, J. Gebhart, G. Rudolf, C. F. Schiller, and W. Stahlhofen. Deposition of particles in the human respiratory tract in the size range 0.005-15 micro m. *Journal of Aerosol Science*, 17:811–825, 1986.

[16] L. M. Hopkins, J. T. Kelly, A. S. Wexler, and A. K. Prasad. Particle image velocimetry measurements in complex geometries. *Experiments in Fluids*, 29:91–95, July 2000.

[17] R. F. Hounam, A. Black, and M. Walsh. Deposition of aerosol particles in the nasopharyngeal region of the human respiratory tract. *Nature*, 221:1254–1255, March 1969.

[18] Central intelligence Agency. The world factbook, life expectancy at birth. *https://www.cia.gov/library/publications/the-world-factbook/rankorder/2102rank.html*, 2007.

[19] D. Isabey and H. K. Chang. Steady and unsteady pressure-flow relationships in central airways. *J Appl Physiol*, 51:1338–1348, November 1981.

[20] H. Itoh, G. C. Smaldone, D. L. Swift, and H. N. Wagner. Mechanisms of aerosol deposition in a nasal model. *Journal of Aerosol Science*, 16:529–534, 1985.

[21] H M Janssens, J C de Jongste, W J Fokkens, S G Robben, K Wouters, and H A Tiddens. The sophia anatomical infant nose-throat (saint) model: a valuable tool to study aerosol deposition in infants. *Journal of aerosol medicine : the official journal of the International Society for Aerosols in Medicine*, 14:433–41, 2001. PMID: 11791684.

[22] Hettie M. Janssens. *Aerosol Therapy in Young Children.* Hettie M. Janssens, 1 edition, October 2001.

[23] Hettie M. Janssens, Johan C. de Jongste, Wim C. J. Hop, and Harm A. W. M. Tiddens. Extra-fine particles improve lung delivery of inhaled steroids in infants: A study in an upper airway model. *Chest*, 123:2083–2088, June 2003.

[24] Hettie M Janssens, Arno Krijgsman, Ton F M Verbraak, Wim C J Hop, Johan C de Jongste, and Harm A W M Tiddens. Determining factors of aerosol deposition for four pmdi-spacer combinations in an infant upper airway model. *Journal of aerosol medicine : the official journal of the International Society for Aerosols in Medicine*, 17:51–61, 2004. PMID: 15120013.

[25] Hettie M Janssens, Els C van der Wiel, Anton F M Verbraak, Johan C de Jongste, Peter J F M Merkus, and Harm A W M Tiddens. Aerosol therapy and the fighting toddler: is administration during sleep an alternative? *Journal of*

aerosol medicine : the official journal of the International Society for Aerosols in Medicine, 16:395–400, 2003. PMID: 14977430.

[26] Satish G. Kandlikar, Derek Schmitt, Andres L. Carrano, and James B. Taylor. Characterization of surface roughness effects on pressure drop in single-phase flow in minichannels. *Physics of Fluids*, 17:100606–11, October 2005.

[27] James Kelly, Bahman Asgharian, Julia Kimbell, and Brian Wong. Particle deposition in human nasal airway replicas manufactured by different methods. part i: Inertial regime particles. *Aerosol Science and Technology*, 38:1063–1071, 2004.

[28] James T Kelly, Bahman Asgharian, and Brian A Wong. Inertial particle deposition in a monkey nasal mold compared with that in human nasal replicas. *Inhalation toxicology*, 17:823–30, December 2005. PMID: 16282160.

[29] Nola J. Kennedy and William C. Hinds. Inhalability of large solid particles. *Journal of Aerosol Science*, 33:237–255, February 2002.

[30] J. S. Kimbell. Nasal dosimetry of inhaled gases and particles: where do inhaled agents go in the nose? *Toxicologic pathology*, 34:270–273, 2006.

[31] Paul A. Baron Klaus Willeke. *Aerosol Measurement: Principles, Techniques, and Applications*. Van Nostrand Reinhold, 1993.

[32] Johannes Lang. *Clinical Anatomy of the Nose, Nasal Cavity and Paranasal Sinuses*. Thieme Medical Publishers, Inc., 1989.

[33] Guillaume Lavoue. A roughness measure for 3d mesh visual masking. *ACM SIGGRAPH Symposium on Applied Perception in Graphics and Visualization*, July 2007.

[34] Yuan Liu, Edgar A. Matida, Junjie Gu, and Matthew R. Johnson. Numerical simulation of aerosol deposition in a 3-d human nasal cavity using rans, rans/eim, and les. *Journal of Aerosol Science*, 38:683–700, July 2007.

[35] Kevin T Morgan and Thomas M Monticello. Airflow, gas deposition, and lesion distribution in the nasal passages. *Environmental Health Perspectives*, 85:209–218, April 1990.

[36] Niels Mygind and Ronald Dahl. Anatomy, physiology and function of the nasal cavities in health and disease. *Advanced Drug Delivery Reviews*, 29:3–12, 1998.

[37] Glasgow College of Nautical Studies. Pipe friction chart. *www.glasgow-nautical.ac.uk*.

[38] T R Rasmussen, A Andersen, and O F Pedersen. Particle deposition in the nose related to nasal cavity geometry. *Rhinology*, 38:102–7, September 2000. PMID: 11072654.

[39] M Rosenthal and A Bush. Ventilatory variables in normal children during rest and exercise. *Eur Respir J*, 16:1075–1083, December 2000.

[40] Hauszermann S, Bailey A. G, Bailey M. R, Etherington G, and Youngman M. The influence of breathing patterns on particle deposition in a nasal replicate cast.

[41] C. T. Sasaki, P. A. Levine, J. T. Laitman, and E. S. Crelin. Postnatal descent of the epiglottis in man. a preliminary report. *Arch Otolaryngol*, 103:169–171, March 1977.

[42] Karen G Schüepp, Juergen Jauernig, Hettje M Janssens, Harm A W M Tiddens, Daniel A Straub, Roland Stangl, Manfred Keller, and Johannes H Wildhaber. In vitro determination of the optimal particle size for nebulized aerosol delivery to infants. *Journal of aerosol medicine*, 18:225–35, 2005. PMID: 15966777.

[43] Scott, Taulbee, and Yu. Theoretical study of nasal deposition. *Bulletin of Mathematical Biology*, 40:581–604, 1978.

[44] D.L. Swift. Inspiratory inertial deposition of aerosols in human nasal airway replicate casts: Implication for the proposed ncrp lung model. *Radiat Prot Dosimetry*, 38:29–34, September 1991.

[45] A Tal, H Golan, N Grauer, M Aviram, D Albin, and M R Quastel. Deposition pattern of radiolabeled salbutamol inhaled from a metered-dose inhaler by means of a spacer with mask in young children with airway obstruction. *The Journal of pediatrics*, 128:479–84, April 1996. PMID: 8618180.

[46] Johannes H. Wildhaber, Hettie M. Janssens, Frédéric Piérart, Nigel D. Dore, Sunalene G. Devadason, and Peter N. LeSouëf. High-percentage lung delivery in children from detergent-treated spacers. *Pediatric Pulmonology*, 29:389–393, 2000.

Appendix A

Raw Data Tables

	SAINT		
$Q\,(cm^3/s)$	$d_a(\mu m)$	Dep	
91.00	0.80	0.01	
112.84	0.80	0.01	
160.66	0.80	0.03	
166.74	0.80	0.03	
185.42	0.80	0.05	
91.00	1.28	0.01	
112.84	1.28	0.02	
160.66	1.28	0.06	
166.74	1.28	0.06	
185.42	1.28	0.10	
91.00	2.03	0.04	
112.84	2.03	0.08	
160.66	2.03	0.17	
166.74	2.03	0.17	
185.42	2.03	0.25	
91.00	3.21	0.13	
112.84	3.21	0.24	
160.66	3.21	0.38	
166.74	3.21	0.38	
185.42	3.21	0.48	
91.00	5.33	0.31	
112.84	5.33	0.46	
160.66	5.33	0.62	
166.74	5.33	0.61	
185.42	5.33	0.70	

Table A.1: Averaged data for SAINT

	Subject 2		
$Q\,(cm^3/s)$	$d_a(\mu m)$	Dep	
92.82	0.80	-0.00	
115.11	0.80	0.00	
163.34	0.80	0.00	
169.91	0.80	0.01	
188.61	0.80	0.01	
92.82	1.28	-0.00	
115.11	1.28	0.00	
163.34	1.28	0.01	
169.91	1.28	0.01	
188.61	1.28	0.02	
92.82	2.03	0.00	
115.11	2.03	0.01	
163.34	2.03	0.02	
169.91	2.03	0.02	
188.61	2.03	0.04	
92.82	3.21	0.02	
115.11	3.21	0.03	
163.34	3.21	0.08	
169.91	3.21	0.08	
188.61	3.21	0.12	
92.82	5.33	0.06	
115.11	5.33	0.10	
163.34	5.33	0.23	
169.91	5.33	0.23	
188.61	5.33	0.31	

Table A.2: Averaged data for Subject 2

75

Subject 3		
$Q\ (cm^3/s)$	$d_a(\mu m)$	Dep
92.08	0.80	0.01
114.02	0.80	0.01
163.19	0.80	0.02
169.33	0.80	0.03
187.19	0.80	0.04
92.08	1.28	0.02
114.02	1.28	0.03
163.19	1.28	0.07
169.33	1.28	0.08
187.19	1.28	0.10
92.08	2.03	0.04
114.02	2.03	0.08
163.19	2.03	0.15
169.33	2.03	0.16
187.19	2.03	0.20
92.08	3.21	0.09
114.02	3.21	0.15
163.19	3.21	0.25
169.33	3.21	0.27
187.19	3.21	0.32
92.08	5.33	0.17
114.02	5.33	0.26
163.19	5.33	0.40
169.33	5.33	0.41
187.19	5.33	0.48

Table A.3: Averaged data for Subject 3

Subject 4		
$Q\ (cm^3/s)$	$d_a(\mu m)$	Dep
91.43	0.80	-0.00
113.57	0.80	0.01
161.66	0.80	0.02
167.82	0.80	0.02
186.49	0.80	0.03
91.43	1.28	0.00
113.57	1.28	0.02
161.66	1.28	0.04
167.82	1.28	0.04
186.49	1.28	0.07
91.43	2.03	-0.02
113.57	2.03	0.05
161.66	2.03	0.13
167.82	2.03	0.12
186.49	2.03	0.19
91.43	3.21	0.09
113.57	3.21	0.17
161.66	3.21	0.32
167.82	3.21	0.32
186.49	3.21	0.42
91.43	5.33	0.25
113.57	5.33	0.39
161.66	5.33	0.57
167.82	5.33	0.57
186.49	5.33	0.66

Table A.4: Averaged data for Subject 4

Subject 5		
Q (cm^3/s)	$d_a(\mu m)$	Dep
91.61	0.80	0.00
113.82	0.80	0.01
160.58	0.80	0.02
166.73	0.80	0.02
186.27	0.80	0.04
91.61	1.28	0.01
113.82	1.28	0.03
160.58	1.28	0.05
166.73	1.28	0.05
186.27	1.28	0.08
91.61	2.03	0.03
113.82	2.03	0.07
160.58	2.03	0.13
166.73	2.03	0.14
186.27	2.03	0.20
91.61	3.21	0.10
113.82	3.21	0.19
160.58	3.21	0.33
166.73	3.21	0.34
186.27	3.21	0.43
91.61	5.33	0.27
113.82	5.33	0.42
160.58	5.33	0.60
166.73	5.33	0.60
186.27	5.33	0.69

Table A.5: Averaged data for Subject 5

Subject 6		
Q (cm^3/s)	$d_a(\mu m)$	Dep
90.49	0.80	0.03
112.81	0.80	0.06
159.10	0.80	0.10
165.26	0.80	0.10
183.52	0.80	0.16
90.49	1.28	0.10
112.81	1.28	0.17
159.10	1.28	0.27
165.26	1.28	0.26
183.52	1.28	0.35
90.49	2.03	0.27
112.81	2.03	0.39
159.10	2.03	0.50
165.26	2.03	0.50
183.52	2.03	0.59
90.49	3.21	0.49
112.81	3.21	0.61
159.10	3.21	0.70
165.26	3.21	0.69
183.52	3.21	0.76
90.49	5.33	0.68
112.81	5.33	0.78
159.10	5.33	0.83
165.26	5.33	0.81
183.52	5.33	0.87

Table A.6: Averaged data for Subject 6

Subject 7		
Q (cm^3/s)	d_a (μm)	Dep
91.22	0.80	0.00
113.72	0.80	0.02
161.15	0.80	0.04
166.56	0.80	0.04
185.68	0.80	0.06
91.22	1.28	0.01
185.68	1.28	0.10
166.56	1.28	0.07
161.15	1.28	0.07
113.72	1.28	0.04
91.22	2.03	0.04
113.72	2.03	0.08
161.15	2.03	0.13
166.56	2.03	0.13
185.68	2.03	0.18
91.22	3.21	0.09
113.72	3.21	0.15
161.15	3.21	0.24
166.56	3.21	0.26
185.68	3.21	0.32
91.22	5.33	0.18
113.72	5.33	0.30
161.15	5.33	0.44
166.56	5.33	0.46
185.68	5.33	0.54

Table A.7: Averaged data for Subject 7

Subject 8		
Q (cm^3/s)	d_a (μm)	Dep
90.64	0.80	0.01
113.41	0.80	0.01
159.09	0.80	0.03
164.87	0.80	0.02
184.73	0.80	0.04
90.64	1.28	0.01
184.73	1.28	0.11
164.87	1.28	0.06
159.09	1.28	0.06
113.41	1.28	0.03
90.64	2.03	0.04
113.41	2.03	0.09
159.09	2.03	0.20
164.87	2.03	0.20
184.73	2.03	0.30
90.64	3.21	0.15
113.41	3.21	0.29
159.09	3.21	0.46
164.87	3.21	0.45
184.73	3.21	0.57
90.64	5.33	0.38
113.41	5.33	0.55
159.09	5.33	0.69
164.87	5.33	0.69
184.73	5.33	0.77

Table A.8: Averaged data for Subject 8

Subject 10		
Q (cm^3/s)	$d_a(\mu m)$	Dep
91.83	0.80	-0.01
114.34	0.80	0.00
163.17	0.80	0.01
169.71	0.80	0.01
188.81	0.80	0.01
91.83	1.28	-0.00
114.34	1.28	0.00
163.17	1.28	0.01
169.71	1.28	0.01
188.81	1.28	0.01
91.83	2.03	-0.00
114.34	2.03	0.00
163.17	2.03	0.02
169.71	2.03	0.01
188.81	2.03	0.02
91.83	3.21	0.01
114.34	3.21	0.02
163.17	3.21	0.04
169.71	3.21	0.04
188.81	3.21	0.06
91.83	5.33	0.03
114.34	5.33	0.05
163.17	5.33	0.12
169.71	5.33	0.12
188.81	5.33	0.18

Table A.9: Averaged data for Subject 10

Subject 11		
Q (cm^3/s)	$d_a(\mu m)$	Dep
89.73	0.80	0.02
112.36	0.80	0.04
159.49	0.80	0.08
164.48	0.80	0.08
183.51	0.80	0.12
89.73	1.28	0.06
112.36	1.28	0.10
159.49	1.28	0.16
164.48	1.28	0.17
183.51	1.28	0.23
89.73	2.03	0.12
112.36	2.03	0.20
159.49	2.03	0.29
164.48	2.03	0.29
183.51	2.03	0.37
89.73	3.21	0.23
112.36	3.21	0.34
159.49	3.21	0.46
164.48	3.21	0.45
183.51	3.21	0.55
89.73	5.33	0.38
112.36	5.33	0.52
159.49	5.33	0.64
164.48	5.33	0.63
183.51	5.33	0.72

Table A.10: Averaged data for Subject 11

Subject 14		
Q (cm^3/s)	$d_a(\mu m)$	Dep
91.57	0.80	-0.01
114.59	0.80	0.00
162.26	0.80	0.01
168.63	0.80	0.00
187.82	0.80	0.01
91.57	1.28	-0.00
114.59	1.28	0.00
162.26	1.28	0.01
168.63	1.28	0.01
187.82	1.28	0.02
91.57	2.03	0.00
114.59	2.03	0.01
162.26	2.03	0.03
168.63	2.03	0.03
187.82	2.03	0.06
91.57	3.21	0.02
114.59	3.21	0.04
162.26	3.21	0.12
168.63	3.21	0.12
187.82	3.21	0.18
91.57	5.33	0.07
114.59	5.33	0.14
162.26	5.33	0.30
168.63	5.33	0.30
187.82	5.33	0.40

Table A.11: Averaged data for Subject 14